

## RESEARCH ARTICLE

# Cockroaches adjust body and appendages to traverse cluttered large obstacles

Yaqing Wang, Ratan Othayoth and Chen Li\*

## ABSTRACT

To traverse complex terrain, animals often transition between locomotor modes. It is well known that locomotor transitions can be induced by switching in neural control circuits or driven by a need to minimize metabolic energetic cost. Recent work revealed that locomotor transitions in complex 3D terrain cluttered with large obstacles can emerge from physical interaction with the environment controlled by the nervous system. For example, to traverse cluttered, stiff grass-like beams, the discoid cockroach often transitions from using a strenuous pitch mode pushing across the beams to using a less strenuous roll mode rolling into and through the gaps. This transition can save mechanical energetic cost substantially ( $\sim 10^0$ – $10^1$  mJ) but requires overcoming a potential energy barrier ( $\sim 10^{-3}$ – $10^{-2}$  mJ). Previous robotic physical modeling demonstrated that kinetic energy fluctuation of body oscillation from self-propulsion can help overcome the barrier and facilitate this transition. However, the animal was observed to transition even when the barrier still exceeded kinetic energy fluctuation. Here, we further studied whether and how the cockroach makes active adjustments to facilitate this transition to traverse cluttered beams. The animal repeatedly flexed its head and abdomen, reduced hindleg sprawl, and depressed one hindleg and elevated the other during the pitch-to-roll transition, adjustments which were absent when running on a flat ground. Using a refined potential energy landscape with additional degrees of freedom to model these adjustments, we found that head flexion did not substantially reduce the transition barrier (by  $\sim 10^{-3}$  mJ), whereas leg sprawl reduction did so dramatically (by  $\sim 10^{-2}$  mJ). We speculate that head flexion is for sensing the terrain to guide the transition via sensory feedback control.

**KEY WORDS:** Terrestrial locomotion, Locomotor transitions, Potential energy barrier, Terradynamics, Kinematics

## INTRODUCTION

Animal locomotion emerges from direct physical interaction with the environment controlled by the nervous system via both feedforward reflexes facilitated by morphology and feedback control modulated by sensing (Dickinson et al., 2000). To move across complex environments, animals often use and transition between multiple modes of locomotion (Alexander, 2002;

Dickinson et al., 2000; Li et al., 2015; Lock et al., 2013; Low et al., 2015). Most terrestrial locomotion studies have focused on how animals use neuromechanical control to generate or stabilize near-steady-state, single-mode locomotion (e.g. walking, running: Blickhan and Full, 1993; Kuo, 2007). Previous work explored how gait transitions result from changes in the rhythmic output of central pattern generators (Ijspeert, 2008), sensed information of the environment (Blaesing and Cruse, 2004; Ritzmann et al., 2012) or the need to minimize metabolic energy cost over large spatiotemporal scales (Bramble and Lieberman, 2004; Shepard et al., 2013).

Recent research in our lab has begun to offer insight into how locomotor transitions can emerge from animals' direct physical interaction with the environment (Gart and Li, 2018; Gart et al., 2018; Han et al., 2021; Li et al., 2015, 2017, 2019b; Othayoth and Li, 2021; Othayoth et al., 2020; Xuan and Li, 2020a,b; Zheng et al., 2022). In particular, these studies have established a potential energy landscape approach to understanding stochastic yet stereotyped animal locomotor transitions in complex 3D terrain with many large obstacles (Othayoth et al., 2020, 2021). In such terrain, physical interaction of the animal with the environment results in a potential energy landscape with distinct basins. Because the animal's self-propulsion breaks continuous frictional terrain contact, the system is statically unstable and drifts down the potential energy basin. This attraction towards distinct landscape basins results in the system having stereotyped locomotor modes. Thus, transitions between locomotor modes can be generated by taking actions to destabilize the system across potential energy barriers separating landscape basins. The barrier height measures the difficulty of making a transition. Most of these studies have focused on how locomotor transitions can be induced by feedforward self-propulsive mechanisms (Gart and Li, 2018; Gart et al., 2018; Han et al., 2021; Othayoth and Li, 2021; Othayoth et al., 2020; Xuan and Li, 2020a,b; Zheng et al., 2022). Not surprisingly, some of them also found evidence that animals can make active adjustments (presumably using sensory feedback control) to aid locomotor transitions (Gart and Li, 2018; Gart et al., 2018; Han et al., 2021; Othayoth et al., 2020).

Here, we took the next step in quantifying and understanding how animals use active adjustments to better make locomotor transitions in complex 3D terrain. Our study was motivated by and built upon a recent study of the discoid cockroach (*Blaberus discoidalis*) traversing a layer of cluttered grass-like beam obstacles (Othayoth et al., 2020). When encountering stiff beams, the animal often first pushes against the beams, resulting in the body pitching up (the pitch mode; Fig. 1, thick blue arrow), but then rolls its body into a gap between beams (the roll mode; Fig. 1, red arrow) to traverse, rarely pushing down the beams to traverse (Fig. 1, thin blue arrow). The animal may also get deflected sideways when exploring in front of the beams (the deflect mode; Fig. 1, purple dashed curve) (Li et al., 2015). Potential energy landscape modeling revealed that

Department of Mechanical Engineering, Johns Hopkins University, Baltimore, MD 21218, USA.

\*Author for correspondence (chen.li@jhu.edu)

 Y.W., 0000-0001-6884-323X; R.O., 0000-0001-5431-9007; C.L., 0000-0001-7516-3646

This is an Open Access article distributed under the terms of the Creative Commons Attribution License (<http://creativecommons.org/licenses/by/4.0>), which permits unrestricted use, distribution and reproduction in any medium provided that the original work is properly attributed.

Received 4 October 2021; Accepted 25 April 2022

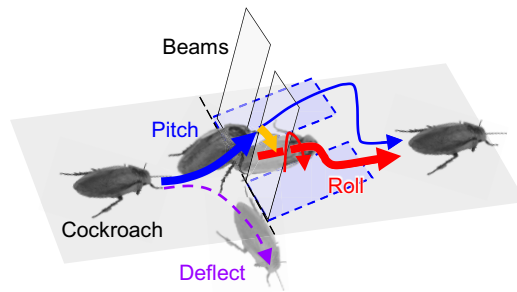


**Fig. 1. Stereotyped pitch and roll modes and pitch-to-roll transition during cluttered grass-like beam traversal of discoid cockroaches.** A possible deflect mode is also shown (see Materials and Methods, ‘Quantifying the difficulty of transition using the potential energy barrier’). Adapted from Othayoth et al. (2020).

the pitch and roll modes emerge as the system is attracted to distinct pitch and roll basins of the potential energy landscape, respectively. Both the pitch and roll modes are more strenuous than running on a flat ground [with a minimal mechanical energetic cost of 7.9 mJ and 0.2 mJ, respectively, for the stiff beams tested in this study; see Supplementary Materials and Methods, ‘Minimal mechanical energetic cost in pitch and roll mode’; these are 130 times and 3 times that needed per stride during medium-speed running at 5 body lengths  $s^{-1}$  (Kram et al., 1997), respectively]. Transition from the pitch to the roll mode can substantially reduce mechanical energy cost (by  $\sim 10^0$ – $10^1$  mJ), but it requires overcoming a potential energy barrier between the pitch and roll basins ( $\sim 10^{-3}$ – $10^{-2}$  mJ; see Supplementary Materials and Methods, Pitch-to-roll transition barrier). Systematic experiments using a feedforward-controlled robot demonstrated that kinetic energy fluctuation from body oscillations resulting from self-propulsion can induce transitions from the pitch to the roll mode (Fig. 1, orange arrow), when it exceeds the potential energy barrier between the pitch and roll basins. However, despite qualitatively similar overall findings, the animal’s pitch-to-roll transition happens even when its body kinetic energy fluctuation is insufficient to overcome the barrier. This means that the animal must also be making active adjustments to facilitate the transition.

To achieve our goal, we challenged the discoid cockroach to traverse a layer of stiff beams and used high-speed imaging to measure detailed body and appendage kinematics during the pitch-to-roll transition. We discovered that the animal made several adjustments. (1) Head flexion: the animal repeatedly flexed its head while interacting with the beams. (2) Abdomen flexion: the animal flexed its abdomen while interacting with the beams and after the animal rolled into the beam gap. (3) Leg sprawl: the animal spread both its hindlegs further outward when pitching against the beams, but tucked one hindleg inward when rolling into the beam gap. (4) Differential leg use: the animal depressed one hindleg (moved the foot further away from the thorax) and elevated the other (moved the foot closer to the thorax) when rolling into the beam gap.

We hypothesized that the animal’s head flexion and leg sprawl adjustment facilitate the pitch-to-roll transition. Specifically: when the animal is pitched up against the beams, (1) head flexion and (2) tucking in the legs reduces the pitch-to-roll transition barrier and facilitates rolling into the gap; and (3) after the animal body has rolled into the gap, head flexion helps it stay in the gap.

To test hypotheses 1 and 2, we used potential energy landscape modeling to analyze whether and how much the observed use of head flexion and leg tucking in changed the potential energy barrier that must be overcome to transition from the pitch to roll mode

(which measures the difficulty of the transition). We found that leg tucking in reduced the pitch-to-roll transition barrier, supporting hypothesis 2, but head flexion did not, rejecting hypothesis 1. To test hypothesis 3, we analyzed whether and how much the observed head flexion changed the potential energy barrier that prevented the animal from transitioning from the rolled body being within the gap between the beams to being out of the gap and deflecting sideways. We found that head flexion did not substantially increase the roll-to-deflect barrier, rejecting hypothesis 3. Finally, we discuss the likely functions of the observed body and appendage adjustments and suggest future directions.

## MATERIALS AND METHODS

We first performed animal experiments and obtained kinematics data (see ‘Animals’ to ‘Statistics’, below). Then, we constructed the potential energy landscape of the system along the observed average trajectory and analyzed cross-sections of the landscape relevant to the animal’s body pitch and roll. We identified local minimum basins corresponding to the pitch and roll modes in the pitch–roll cross-section. Next, we identified saddle points between the pitch and roll basins, and quantified the potential energy barrier (see ‘Potential energy landscape model definition’, ‘Potential energy landscape generation’, and ‘Quantifying the difficulty of transition using the potential energy barrier’, below). Finally, we varied head flexion and total sprawl of the two hindlegs and assessed how the barrier changed compared with that using the constant average values to test hypotheses 1 and 2 about the functions of head and leg adjustments during the pitch-to-roll transition (see ‘Testing the usefulness of head flexion’ and ‘Testing the usefulness of leg tucking in’, below). We also performed these analyses on a yaw cross-section of the landscape (see ‘Quantifying the difficulty of transition using the potential energy barrier’, below) to test hypothesis 3 about the function of head adjustment to keep the animal within the beam gap (see ‘Testing the usefulness of head flexion’, below).

## Animals

We used three adult male cockroaches (*Blaberus discoidalis* Audinet-Serville 1839) (Joe’s BUGz LLC, Atlanta, GA, USA). Before the experiments, each animal was kept in a plastic container in a room with a controlled temperature of 22°C, moisture of 70%, and lighting on a 12 h:12 h light:dark cycle. Dry dog food (Purina Beneful, Largo, FL, USA) and water jelly made from water and polymer crystal (Tasty Worms Nutrition Inc.) were provided *ad libitum*. The animals weighed  $2.7 \pm 0.6$  g (with marker items) and measured  $5.3 \pm 0.3$  cm in length,  $2.3 \pm 0.1$  cm in width and  $0.73 \pm 0.08$  cm in thickness. All data reported are means  $\pm$  s.d.

## Obstacle track

For controlled, repeatable experiments, we constructed a testbed (Fig. 2A) similar to that in our previous study (Othayoth et al., 2020), with a layer of seven beam obstacles. Each beam was 10 mm wide, 100 mm tall and 0.8 mm thick. The lateral distance between two adjacent beams was 10 mm, and the lateral distance between the left-/right-most beams and the walls was 5 mm. We used the same method to construct beam obstacles and characterize their stiffness as that described in our previous study (Othayoth et al., 2020). The beams can only deflect about a hinge just above the ground. The beam torsional stiffness was  $K = 2.5 \pm 0.4$  mN m  $rad^{-1}$  (mean  $\pm$  s.d. of 7 loading cycles), which was between the two most stiff beams in the previous study. We chose this high stiffness to induce a high pitch-to-roll transition probability (Othayoth et al., 2020) to increase experimental yield.

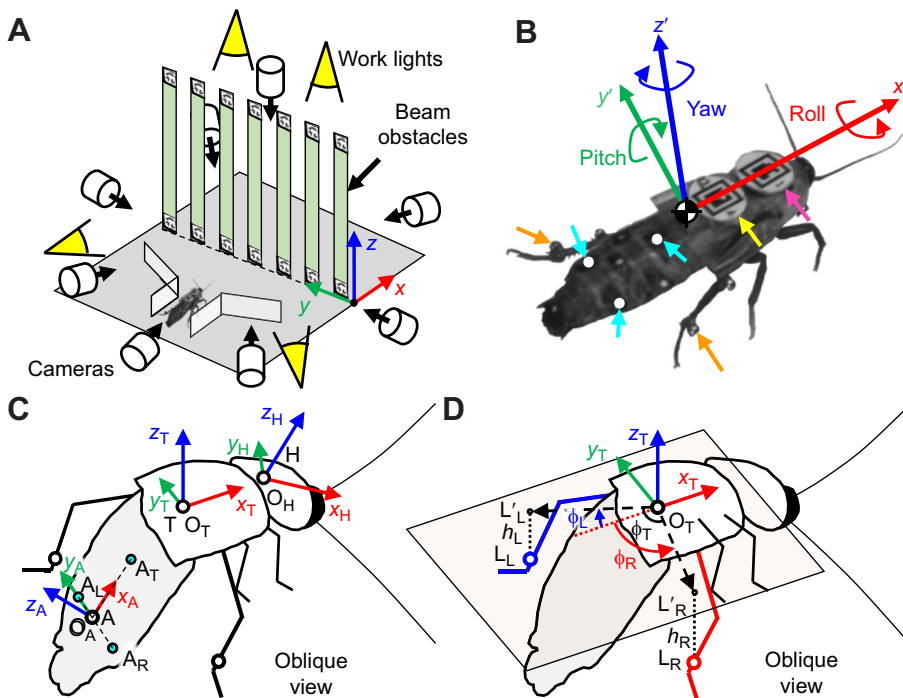


**Fig. 2. Experimental setup and cockroach schematic diagrams.** (A) Schematic diagram of the beam obstacle track and multi-camera imaging system. (B) Marker placement on the animal and definition of body (thorax) frame. Magenta: head marker. Yellow: thorax marker. Cyan: abdomen markers. Orange: leg markers. (C) Definition of thorax, head and abdomen frames. Coordinate  $X_T Y_T Z_T$ : body (thorax) frame. Coordinate  $X_H Y_H Z_H$ : head frame. Coordinate  $X_A Y_A Z_A$ : abdomen frame. (D) Definition of leg sprawl and leg height. Light-colored plane: body coronal plane.  $L_L$ : left leg marker.  $L_R$ : right leg marker.  $L'_L, L'_R$ : projections of leg markers on the body coronal plane.  $\phi_L$ : left leg sprawl angle.  $\phi_R$ : right leg sprawl angle.  $\phi_T$ : total leg sprawl angle.  $h_L$ : left leg height.  $h_R$ : right leg height. A negative leg height means the leg marker is below the thorax coronal plane, and a positive leg height means the leg marker is above it.

### Imaging setup

Eight synchronized high-speed cameras (N5A-100, Adimec, Eindhoven, The Netherlands) recorded the experiment from different views: one from the top view, two from the side view, one from the top-down oblique view, and four from isometric views (Fig. 2A). All the cameras recorded at a frame rate of 100 Hz, a shutter time of 50  $\mu$ s and a resolution of 2592 $\times$ 2048 pixels. Even with eight cameras, we had to carefully tune camera positioning and orientation to achieve reliable tracking of the animal and beams (see ‘Tracking and 3D reconstruction’, below), because the animal had large 3D body rotations (maximum absolute yaw 100 deg, maximum absolute pitch 62 deg, maximum absolute roll 98 deg; defined in ‘Kinematics and kinetic energy fluctuation analyses’, below) and markers were frequently occluded by the beams. Four halogen work lights (Coleman Cable, Waukegan, IL, USA) provided lighting from the top and side. During experiments, the ambient temperature around the arena was around 36°C. To prevent the cockroaches from overheating, we turned off the work lights between trials.

### Experiment protocol

During each trial, we first placed the animal at the start of the track, covered it with a piece of cardboard, and let it settle down. We recorded the ambient temperature around the obstacle field and reset the beams upright. Then we started camera recording, lifted the cardboard to expose the animal to bright light, and prodded its abdomen with a tape-wrapped straw to induce running through the funnel towards the beams. After the animal traversed the beams, it entered a shelter of egg cartons (not shown in Fig. 2A) at the other end of the track. Then, camera recording was stopped, and videos were saved. The animal was allowed at least 3 min to rest after each trial. For each of the three animals tested, we recorded 18–19 trials.

For each animal, we rejected the trials in which at least one of the following situations occurred. (1) The animal used at least one locomotor mode (Li et al., 2015) other than the pitch and roll modes (Othayoth et al., 2020) to traverse the beams. (2) The animal touched the arena wall in the roll phase (defined in ‘Definition of

traversal phases’, below). (3) At least one marker (BEEtags, white-outs or beads) fell off. From the remaining trials, we selected the 12 trials with the shortest traversal time for each of the three animals tested, with a total of 36 trials. This sample downsizing was done because of the significant time cost of digitizing (see next section).

### Tracking and 3D reconstruction

To overcome the challenge of tracking from large 3D body rotation and frequent occlusions, we used several types of markers (Fig. 2B). (1) We glued the animal’s wings into a natural folded shape using hot glue and exposed the abdomen by trimming the posterior half of the wings. Then we used hot glue to attach a BEEtag (Crall et al., 2015) to the anterior half of the fixed wings covering the thorax as the thorax marker (Fig. 2B, yellow). (2) We used hot glue to attach a BEEtag onto the animals’ pronotum as the head marker (Fig. 2B, magenta). (3) We used white-out to paint point markers on the dorsal surface of the abdomen as abdomen markers (Fig. 2B, cyan). We did not use BEEtags to track the abdomen, because they often fell off when the animal interacted with the beams with large abdomen flexion. (4) We used ultraviolet curing glue (Bondic, Aurora, ON, Canada) to attach two small, lightweight (12 mg each, 0.4% body mass, 15% hindleg mass; Kram et al., 1997) aluminium beads (McMaster-Carr, Elmhurst, IL, USA) to each hindleg at two locations close to the femoral-tibial and tibial-tarsal joints as leg markers (Fig. 2B, orange). (5) We attached BEEtags (Crall et al., 2015) to the top and the bottom of each beam’s frontal side as beam markers (Fig. 2A). The added mass from the BEEtags (1 mg, 0.03% body mass) was comparable to or less than that of backpacks used in previous studies of dynamic locomotion of discoid cockroaches (e.g. 0.8 $\times$  body mass: Spence et al., 2010; 1.1 $\times$  body mass: Han et al., 2021; 5.2 $\times$  body mass: Jindrich and Full, 2002). We attached all BEEtags and beads under room temperature without cold anesthetizing the animal, because both the hot glue and ultraviolet curing glue used could solidify within a few seconds. We verified that these additional modifications did not significantly affect the animal’s traversal performance and behavior compared with our previous study (Othayoth et al., 2020) where only one BEEtag was

attached to the wings (see Results, ‘Similar overall performance and behavior to previous study’).

Then, we tracked the markers on the animal and beams in each recorded video from all eight cameras. We tracked all the BEEtag markers automatically using a customized MATLAB code modified from the BEEtag master code (Crall et al., 2015). To track the abdomen and leg markers efficiently, we used DeepLabCut (<http://www.mackenziemathislab.org/deeplabcut>; Mathis et al., 2018). For each camera view, we first manually digitized these markers in 10 trials, with 100 video frames from each camera view, and used these data as a training sample to train the neural network. After training, DeepLabCut tracked the markers in these videos. We then visually examined the sample tracking results, manually fixed obvious tracking errors, and re-trained the training sample. After several cycles of manual corrections and reinforcement learning, DeepLabCut could automatically track markers in all videos with high accuracy. We visually checked the tracking result carefully and manually corrected the remaining tracking errors. Using this tracking method, we achieved a high marker tracking performance: the head, thorax, abdomen and leg markers were all tracked in 100% of all the frames of all trials. We emphasize that, even with eight cameras covering a large angular range and using DeepLabCut, tracking detailed kinematics in such a densely cluttered terrain is a very laborious and time-consuming process, because of the large body rotation in 3D and frequent occlusion of markers. In total, it took an experienced experimenter 20 h of manual digitizing, 72 h of automatic tracking, followed by another 150 h of manual correction, to track 36 trials averaging 280 frames each with eight camera views.

Finally, we reconstructed 3D kinematics of all tracked markers using the direct linear transformation method and DLTdv digitizing tool (<https://biomech.web.unc.edu/dltdv/>; Hedrick, 2008). To facilitate 3D calibration, we built a calibration object with 60 BEEtag markers using Lego bricks (The Lego Group, Billund, Denmark).

### Kinematics and kinetic energy fluctuation analyses

With the 3D reconstruction of tracked markers, we quantified the motion of the animal’s head, thorax, abdomen and two hindlegs. For simplicity, we laterally mirrored kinematic data of the trials in which the animal rolled to the left (negative body roll) to become rolling to the right (positive body roll) to simplify the analysis, considering lateral symmetry.

We first approximated the thorax frame (which is the body frame in Othayoth et al., 2020) and head frame using the BEEtags on them. To do this, we projected a model of the animal (see ‘Potential energy landscape model definition’, below) to a set of eight synchronized camera views and adjusted its pose to visually match it to the animal figure in the video. We checked this matching between the model and the animal figure in at least five other frames in the videos. Then we defined the animal’s thorax frame ( $X_T Y_T Z_T$ ) and head frame ( $X_H Y_H Z_H$ ) as the model’s thorax frame and head frame, respectively, and used homogeneous transformation between the tags and the models to represent the spatial relationship between the tags and the animal’s thorax and head. For the abdomen frame ( $X_A Y_A Z_A$ ), we defined the origin ( $O_A$ ) as the foot of the perpendicular from the top marker ( $A_T$ ) to the segment of left ( $A_L$ ) and right markers ( $A_R$ ), defined the  $x$ -axis as the direction from the origin ( $O_A$ ) pointing at the top marker ( $A_T$ ), and defined the  $y$ -axis as the direction from the origin ( $O_A$ ) pointing at the left marker ( $A_L$ ) (Fig. 2C). Thus, we obtained the head, thorax and abdomen frames, each with 3D position ( $x, y, z$ ) and orientation (yaw  $\alpha$ , pitch  $\beta$ , roll  $\gamma$ ,  $Z$ – $Y'$ – $X''$

Tait–Bryan convention) (Fig. 2C). Note that a negative pitch angle means the body is pitched up.

We then calculated the following kinematic variables as a function of time in each trial. (1) Head flexion  $\beta_h$ : the pitch of the head frame in the thorax frame. (2) Abdomen flexion  $\beta_a$ : the additive inverse of the pitch of the abdomen frame in the thorax frame. The additive inverse (positive becoming negative, and negative becoming positive) was used so that  $\beta_a$  is positive when the animal flexes the abdomen down. (3) Leg sprawl  $\phi_L, \phi_R, \phi_T$ : the angle from the vector from the thorax frame origin ( $O_B$ ) to the leg markers’ projection into the body coronal plane ( $L'_L, L'_R$ ) to the  $x$  direction of thorax frame is defined as left and right leg sprawl angle ( $\phi_L, \phi_R$ ), respectively. Total leg sprawl  $\phi_T$  is the sum of the two (Fig. 2D). (4) Leg height difference  $\Delta h$ : the leg height of the right hindleg ( $h_R$ ) minus the leg height of the left hindleg ( $h_L$ ) (after mirroring). Hindleg height was defined as the distance of the leg marker from the thorax coronal plane (Fig. 2D). A negative leg height means that the leg marker is below the thorax coronal plane, and a positive leg height means that it is above. All the equations are summarized below.

The rotation matrix of the thorax ( $R_T$ ), head ( $R_H$ ) and abdomen ( $R_A$ ) frames from the world frame can be calculated as:

$$R = \begin{bmatrix} c_\alpha c_\beta & c_\alpha s_\beta s_\gamma - s_\alpha c_\gamma & c_\alpha s_\beta c_\gamma + s_\alpha s_\gamma \\ c_\alpha s_\beta & c_\alpha s_\beta s_\gamma + s_\alpha c_\gamma & c_\alpha s_\beta c_\gamma - s_\alpha s_\gamma \\ -s_\beta & c_\beta s_\gamma & c_\beta c_\gamma \end{bmatrix}, \quad (1)$$

where  $s_\alpha, s_\beta, s_\gamma$  and  $c_\alpha, c_\beta, c_\gamma$  are abbreviations for sine and cosine terms, respectively, and  $\alpha, \beta$  and  $\gamma$  are the Euler angles (yaw, pitch and roll).

The rotation matrix of head and abdomen frames from the thorax frame can be calculated as:

$$\begin{aligned} R_{TH} &= R_T^T R_H, \\ R_{TA} &= R_T^T R_A. \end{aligned} \quad (2)$$

where superscript T represents the transpose of the matrix.

The head flexion and abdomen flexion:

$$\begin{aligned} \beta_h &= \beta(R_{TH}), \\ \beta_a &= -\beta(R_{TA}), \end{aligned} \quad (3)$$

where  $\beta(\cdot)$  means obtaining the pitch of a rotational matrix:

$$\beta(R) = \text{atan2}\left(\sqrt{r_{31}^2 + r_{32}^2}, r_{33}\right), \quad (4)$$

where  $r_{ij}$  is the  $i$ th row, the  $j$ th column element in the matrix  $R$ .

Leg sprawl:

$$\begin{aligned} \phi_L &= \text{sign}[y_T(\overrightarrow{O_T L'_L})] \cdot \cos^{-1}\left[\frac{(\overrightarrow{O_T L'_L} \cdot \overrightarrow{x_T^-})}{\|\overrightarrow{O_T L'_L}\|}\right], \\ \phi_R &= -\text{sign}[y_T(\overrightarrow{O_T L'_R})] \cdot \cos^{-1}\left[\frac{(\overrightarrow{O_T L'_R} \cdot \overrightarrow{x_T^-})}{\|\overrightarrow{O_T L'_R}\|}\right], \\ \phi_T &= \phi_L + \phi_R, \end{aligned} \quad (5)$$

where  $y_T(\cdot)$  means obtain the  $y$  element of a vector in the frame ( $X_T Y_T Z_T$ ), and  $\overrightarrow{x_T^-}$  means the unit vector along  $x_T$  in the negative direction.

Leg height difference:

$$\Delta h = h_R - h_L. \quad (6)$$

To obtain average kinetic energy fluctuation, we first calculated the time average of the animal’s kinetic energy due to translational and

rotational velocity components other than the forward velocity (Othayoth et al., 2020) in the explore+pitch and roll phases for each trial, then averaged the means of all trials. Kinetic energy fluctuation  $\Delta E_K$  was calculated as:

$$\begin{aligned}\Delta E_K &= \frac{1}{2}(mv_y^2 + mv_z^2 + I_{xx}\omega_x^2 + I_{yy}\omega_y^2 + I_{zz}\omega_z^2) \\ &= E_K - \frac{1}{2}mv_x^2,\end{aligned}\quad (7)$$

where  $m$ ,  $I_{xx}$ ,  $I_{yy}$ , and  $I_{zz}$  are mass and moment of inertia along the  $x$ -,  $y$ - and  $z$ -axes,  $v_x$ ,  $v_y$ ,  $v_z$ ,  $\omega_x$ ,  $\omega_y$ ,  $\omega_z$  are the translational and rotational velocities along the  $x$ -,  $y$ - and  $z$ -axes, and  $E_K$  is the animal's total kinetic energy.

During experiments, the animal's hindlegs moved at  $0.17 \pm 0.05 \text{ m s}^{-1}$  (temporal average across all trials), resulting in an estimated kinetic energy of  $0.005 \pm 0.003 \text{ mJ}$  from both hindlegs. We neglected this contribution because it was much smaller than the potential energy barrier reduction from leg flexion ( $0.06 \text{ mJ}$ ; see Results, 'Leg sprawl adjustments facilitate body rolling').

### Definition of traversal phases

To compare the animal's motion in different stages of the traversal, we divided each trial into five distinct phases. (1) Approach: from when the animal ran into the camera view to when it collided with the beams. (2) Explore+pitch: from when the animal collided with the beams to when it started the final, successful roll attempt. Because the animal sometimes attempted to roll its body more than once, here we separated this phase and the next phase with the start of the last, successful attempt. The start of an attempt was defined as the instance when the animal's body roll changed sign from negative to positive (after mirroring; see 'Kinematics and kinetic energy fluctuation analyses', above). (3) Roll: from when the animal started the final, successful body roll attempt to when body roll was maximal. (4) Land: from when body roll was maximal to when the animal landed with all its six legs touching the ground again. (5) Depart: from when the animal landed with all its six legs touching the ground to when it exited the camera views.

Note that the pitch+explore and roll phases here are not the same as the pitch and roll modes in our previous study (Othayoth et al., 2020); instead, these two phases and the subsequent land phase are consecutive stages of the overall process of the animal transitioning from the pitch to the roll mode. The approach and depart phases correspond with the animal running on a flat ground.

Our goal was to quantify and understand what adjustments the animal made to facilitate the pitch-to-roll transition. To achieve this, we focused on analyzing whether there were significant changes in kinematics in the explore+pitch and roll phases, compared with the approach and depart phases. We did not focus on analyzing the complex kinematics in the land phase because the pitch-to-roll transition was completed by then.

### Statistics

To compare across traversal phases, for each trial, we averaged most kinematic variables (body roll  $\gamma$ , body pitch  $\beta$ , total leg sprawl  $\phi_T$  and leg height difference  $\Delta h$ ) over time in each phase. For head flexion  $\beta_h$  and abdomen flexion  $\beta_a$ , for each trial, we instead calculated their standard deviation in each phase. This was because the animal often repeatedly flexed its head and abdomen (see Results, 'Head flexion' and 'Abdomen flexion'), and the head and abdomen flexion angles each often nearly cancelled themselves out when being averaged over time. In contrast, their standard deviation

better reflected the animal's repeated head and abdomen flexion amplitudes.

Then, we pooled the averages of most kinematic variables and standard deviations of head flexion and abdomen flexion from all trials. Using these data, for each pair of phases, we performed a mixed-effects ANOVA, with the phase as a fixed factor and the individual as a random factor to account for individual variability, to determine whether there was a significant difference between phases. These data are reported as means  $\pm$  s.d. across trials (see Results, from 'Body rotations' to 'Leg adjustments').

To check whether the animal's overall performance and behavior in this study were similar to those in our previous study (Othayoth et al., 2020), we performed a fixed-effects ANOVA, with whether the data were from this study or the previous study as the factor, and traversal time and maximal body roll as the variables (see Results, 'Similar overall performance and behavior to previous study').

Because the duration of each phase in each trial varied substantially, plotting kinematics of all the trials as a function of time results in substantial overlap of data of different phases and obscures the trends of kinematics during each phase. To better visualize how body, head, abdomen and leg kinematics change during each phase for each trial, we offset the time of each phase to zero at its beginning and then normalized it to the duration of the phase to be a percentage of each phase. In this way, we aligned the beginning and end of each phase across all the trials. This time normalization allowed clear visualization of the trends of the kinematics and did not affect the results of any other analysis.

All analyses except for statistical tests were performed using MATLAB (MathWorks, Inc., Natick, MA, USA). All statistical tests were performed using JMP 16 (SAS Institute Inc., Cary, NC, USA).

### Potential energy landscape model definition

In our previous study, to generate the potential energy landscape, the animal body was modeled as a single rigid body (Othayoth et al., 2020). Here, to further study how the active adjustments facilitated beam traversal, we refined the animal body model to consist of a head, a thorax and an abdomen (Fig. 3A). Antennas, front and middle legs, and other body parts were neglected (totaling 7% body mass). The hindlegs were neglected (6% body mass) when studying the usefulness of head flexion (see 'Testing the usefulness of head flexion', below), considering that they are not in contact with beams when the pitch-to-roll transition happened. The hindlegs were added when studying the use of leg adjustments (see 'Testing the usefulness of leg tucking in', below). The thorax was modeled as a half-ellipsoid (Fig. 3A, orange; length: 19.9 mm, width: 27.6 mm, thickness: 6.4 mm). The head was modeled as a massless ellipsoid-like rigid body (Fig. 3A, red; length: 9.1 mm, width: 14.4 mm, thickness: 6.0 mm). The abdomen was modeled as half of an ellipsoid (Fig. 3A, yellow; length: 30.5 mm, width: 20.6 mm, thickness: 6.5 mm). All the dimensions above were averages of the measured animal dimensions. When added, the hindlegs were modeled as rigid rods with one side fixed to the thorax center (Fig. 3A, blue and red lines with circle for left and right legs, respectively), because we only tracked the tibial-tarsal joint of the legs. The length of each leg was 27 mm (the average maximal leg length was  $27 \pm 2 \text{ mm}$  in the explore+pitch and roll phases over all trials). For simplicity, we assumed that the head and abdomen could each only flex about a lateral axis fixed to the thorax (i.e. only the pitch degree of freedom was allowed). We set the body center of mass at the middle of the rotation axes between the thorax and the abdomen, which is a reasonable approximation (Kram et al., 1997).

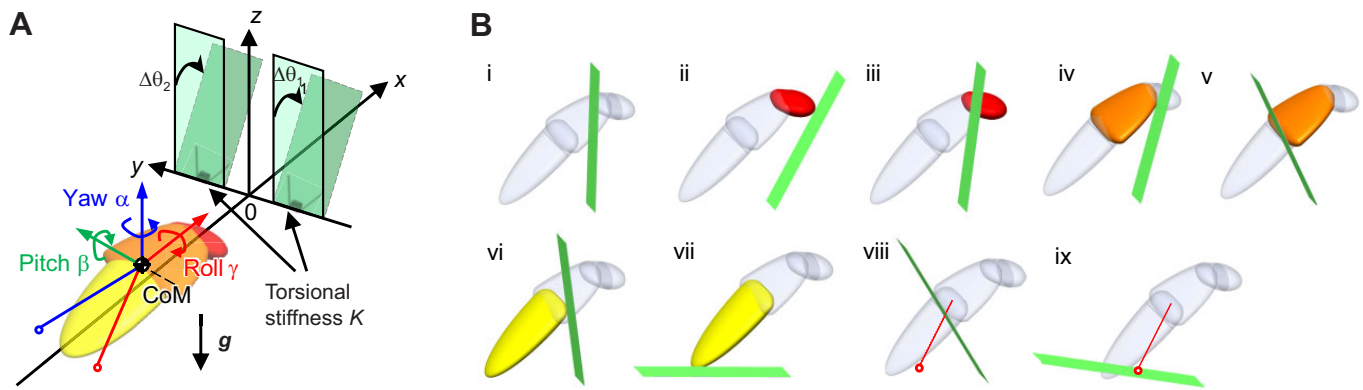


**Fig. 3. System modeling for potential energy landscape approach.** (A) Model of animal and beams and definition of variables. (B) Schematic examples showing the multiple possibilities for beam deflection. Hindlegs (blue and red segments originating from the center of mass (CoM) in A, red segments in Bviii,ix are neglected for analyses on head flexion (Material and Methods, ‘Testing the usefulness of head flexion’; Fig. S1A) and are only included in analyses on leg adjustments (Material and Methods, ‘Testing the usefulness of leg tucking in’; Fig. S1B).

We intentionally designed the overlap between the thorax and the head or abdomen (Fig. 3A; Fig. S1A) to reduce unrealistic concavity between these segments.

The beams were modeled as rigid rectangular plates attached to the ground with Hookean torsional joints at the bottom. Their orientations without animal interaction were set to vertical (Fig. 3A, green with solid contour). In our previous study, the beams were only allowed to deflect forward, and the largest possible deflection angle was always selected (Othayoth et al., 2020). This resulted in overestimated beam deflection. In particular, when the cockroach had already traversed the beams using the roll mode, the estimated beam deflections were still calculated as if the beams blocked in front of the cockroach when the animal used a pitch mode. Here, to refine the model, we allowed the beams to deflect either forward or backward during the interaction, and we determined each beam’s deflection ( $\Delta\theta_1$ ,  $\Delta\theta_2$ ) as the angle with minimal absolute value at which the beam did not overlap with any part of the animal. This revised protocol ensured that, when the cockroach was sufficiently far away from the beam, either not having entered the beam area or having already traversed it, beam deflection was zero; when the animal was interacting but had not traversed the beams, the beams deflected forward; and when the animal had traversed the beams, the beams deflected backward. Note that this revised protocol does not affect the transition barrier analysis, because the pitch-to-roll transition happened when the animal body was only beginning to enter the gap (average body  $x = -13.6 \pm 4.4$  mm when the pitch-to-roll transition happened over all trials); in that case, the two protocols gave the same result.

Below we give an example of how to determine beam deflection (Fig. 3B). When hindlegs were neglected, we first identified seven possible deflection angles, i.e. 0 deg deflection (Fig. 3Bi), deflections where the beam was tangential to the head in the front or back (Fig. 3Bii,iii), to the thorax in the front or back (Fig. 3Biv,v), or to the abdomen in the front or back (Fig. 3Bvi,vii). Sometimes, there were no deflections where the beam was tangential to any body part; in that case, the two possible deflection angles where the beam was tangential to this part were set to be 0 deg. Then, we rejected the beam deflections where the beam overlapped with any body part (Fig. 3Bi,iii,iv,v,vi), and finally selected the deflection angle with minimal absolute value (Fig. 3Bii is selected, Fig. 3Bvii is rejected). When the hindlegs were added for analyzing the function of leg adjustments (see ‘Testing the usefulness of leg tucking in’, below;

Fig. S1B), compared with that neglecting hindlegs, two additional possible deflection angles were identified for each hindleg, i.e. deflections where the beam contacts the leg in the front or back (Fig. 3Bviii,ix, with only the right leg shown for simplicity). The remaining procedure was the same as that neglecting the hindlegs. Beam deflection calculated from this method better matched experimental measurements than in the previous study (Othayoth et al., 2020), reducing the error from  $15 \pm 32$  deg to  $-1 \pm 13$  deg ( $P < 0.001$ , repeated-measures ANOVA).

The potential energy of the system  $E_p$  is the sum of animal and beam gravitational potential energy and beam elastic energy:

$$E_p = m_c g z + m_b g \frac{L}{2} (\cos \Delta\theta_1 + \cos \Delta\theta_2) + \frac{1}{2} K (\Delta\theta_1^2 + \Delta\theta_2^2), \quad (8)$$

where  $m_c$  is the animal mass,  $g$  is gravitational acceleration,  $z$  is the height of the body center of mass from the ground,  $m_b$  is the beam mass,  $L$  is the beam length,  $K$  is the beam torsional stiffness, and  $\Delta\theta_1$  and  $\Delta\theta_2$  are beam deflection from vertical. Given the constraints above, it was fully determined by the animal’s position, orientation, and head and abdomen flexion and did not depend on the trajectory (i.e. determined by configuration with no history dependence). This is crucial for applying the potential energy landscape approach, because it simplifies the problem to be within a finite number of dimensions and further makes the variation of variables practical.

### Potential energy landscape generation

We generated the potential energy landscape similarly to our previous study (Othayoth et al., 2020). The model system has eight degrees of freedom, including the animal position (forward  $x$ , lateral  $y$ , vertical  $z$ ) and orientation (yaw  $\alpha$ , pitch  $\beta$ , roll  $\gamma$ ) of the thorax and head ( $\beta_h$ ) and abdomen ( $\beta_a$ ) flexion. So, the potential energy of the system should be a function of these eight independent variables:

$$E_p = E_p(x, y, z, \alpha, \beta, \gamma, \beta_h, \beta_a). \quad (9)$$

We calculated the potential energy landscape over the 8D space by varying these eight variables: their ranges and increments are listed in Table S1. We did not vary the abdomen flexion  $\beta_a$  for two reasons. First, the head and leg adjustments likely facilitated transition to the roll mode, whereas the abdomen interacted with the beams after the body had already rolled into the gap and likely contributed less to this transition. Second, adding one more

dimension to our potential energy landscape calculations was computationally costly. The first seven dimensions that we varied systematically already took 3 weeks of computation on a 32-core 2.93 GHz workstation. It would take  $\sim 20$  times more (approximately a year) if we varied abdomen flexion like head flexion. To simplify landscape analysis, we focused on two cross-sections of the entire 8D landscape by collapsing less relevant dimensions. We first collapsed the landscape along the  $z$  dimension. For each combination of the other seven variables, potential energy is a function of  $z$ . We varied  $z$  from  $z_{\min}$  (when the body touched the ground) to  $z_{\min}+15$  mm and chose the  $z$  value for which potential energy is minimal, assuming that the unstable (due to self-propulsion) system was attracted to the local minimum. This method was different from that used in our previous study (Othayoth et al., 2020), where the animal's lowest point was constrained to always touch the ground (i.e. ground contact constraint). The body  $z$  obtained from this refined method better matched observations: with the ground contact constraint, to reach the average measured  $z$  when the animal interacted with the beams ( $x=-9$  to  $-3$  mm; Fig. S2B) would require the animal to pitch up by an average of 20 deg, much greater than the observation ( $<10$  deg; Fig. S2D), which was only possible without the ground contact constraint.

Next, we collapsed the landscape along other less relevant dimensions by analyzing landscape cross-sections that follow the average animal trajectory. To extract an average animal trajectory as a function of forward position  $x$ , we first discretized  $x$  within  $[-26$  mm,  $33$  mm] into 296 bins, each spanning 0.2 mm. We checked whether the animal passed any of these  $x$  bins between each two adjacent time steps in each trial. For each bin where this occurred, we determined the values of kinematic variables other than  $x$  using linear interpolation over  $x$  and recorded them under this bin. Finally, we averaged these recorded variables for each  $x$  bin, the evolution of which over  $x$  gave the average animal trajectory (Fig. S2). For the pitch–roll cross-section analysis, we always kept body  $y$  and yaw  $\alpha$  to follow the average trajectory. For the yaw cross-section analysis below, we always kept body  $y$ , body pitch  $\beta$  and roll  $\gamma$  to follow the average trajectory. For both analyses, we constrained the abdomen pitch  $\beta_a$  fixed at 7 deg (temporal average of abdomen flexion was  $\beta_a=7\pm 4$  deg in the approach phase over all trials). When studying the usefulness of head flexion,  $\beta_h$  was kept as a variable (see ‘Testing the usefulness of head flexion’, below). When studying the usefulness of leg tucking in,  $\beta_h$  was set to follow the average trajectory (see ‘Testing the usefulness of leg tucking in’, below). See Table S1 for a summary of the ranges and increment of parameter variation and dimension collapsing protocol.

To study how the head and leg adjustments affected the pitch-to-roll transition (see ‘Testing the usefulness of head flexion’ and ‘Testing the usefulness of leg tucking in’, below), we extracted a pitch–roll cross-section of the landscape, where potential energy is a function of body pitch  $\beta$  and roll  $\gamma$ . In addition, to study whether the head flexion helped the animal stay within the gap after the animal rolled (see ‘Testing the usefulness of head flexion’, below), we extracted a body yaw cross-section of the landscape, where potential energy is a function of body yaw  $\alpha$ .

### Quantifying the difficulty of transition using the potential energy barrier

To transition from one mode to another, the animal had to overcome a potential energy barrier (i.e. transition barrier) on the landscape cross-section. A higher transition barrier means that it is more difficult to transition. We can measure whether and how the

transition barrier changed with an observed adjustment (i.e. head flexion, leg tucking in) to evaluate whether it facilitated or hindered a transition. To quantify the difficulty of transitioning between two modes (i.e. from the pitch to the roll mode, from the roll to the deflect mode), for each  $x$  position during traversal ( $[-26$  mm,  $33$  mm]), we generated the relevant cross-section of the landscape, identified the basins corresponding to the two modes, and calculated the transition barrier.

First, we looped through all points on the landscape to identify the local minima and their basins corresponding to the locomotor modes. To quantify the pitch-to-roll transition barrier, on the pitch–roll landscape cross-section, we located the pitch minimum (Fig. 4B, blue point) with a finite body pitch and a body roll near 0 deg (Fig. 4Ai–iii) and the roll minimum (Fig. 4B, red point), with a body pitch near 0 deg and a body roll around 90 deg (Fig. 4Aiii'). When no roll minimum existed (i.e. when the animal was far from the beams; Fig. 4Bi), we defined (pitch, roll)=(0 deg, 90 deg) as the roll minimum.

To quantify the roll-to-deflect barrier, on the yaw landscape cross-section, we located the roll minimum (Fig. 4D, red point), which corresponded to the body rolled into the gap with a body yaw around 0 deg (Fig. 4Ci,ii), and the two deflect minima (Fig. 4D, purple points), which corresponded with the body deflected towards the left or right with a body yaw around  $\pm 90$  deg (Fig. 4Cii',ii"). Note that the same roll mode (Fig. 4Aiii',Ci,ii) corresponded with the roll basin on the pitch–roll cross-section and the roll basin on the yaw cross-section, which appeared as different basins. This is because the potential energy landscape exists in a high-dimensional space, with 5 degrees of freedom ( $x$ ,  $y$ , pitch, roll, yaw) when not considering head, abdomen and leg adjustments. At the same ( $x$ ,  $y$ ), the same roll basin in the higher-dimension pitch–roll–yaw landscape cross-section appears as different basins on the lower-dimension pitch–roll cross-section and yaw cross-section.

Once we located the pitch and roll basins on the pitch–roll cross-section and roll and deflect basins on the yaw cross-section, we used a breadth-first search to calculate the transition barrier from one basin to another. Breadth-first search is a computational algorithm for searching on graph data structure (Cormen et al., 2009). We fed the gridded potential energy landscape cross-section as the graph data, with the starting minimum as the start point, the destination minimum as the goal point, and the highest potential energy on the traversing route as the cost function. In the breath-first search algorithm, each searched point remembered its parent (the point that this point was developed from), so tracing the parent and further ancestors from the goal point (i.e. parent backtracking) gave an imaginary route from the start to the destination minimum that crossed the lowest energy barrier (Fig. 4B,D, green curve). We defined the point with the highest energy on this route as the saddle point (Fig. 4B,D, orange points on the cross-sections). Note that this ‘saddle point’ is only a true saddle point on the 2D pitch–roll cross-section and when both the pitch and roll minima are actual local minima on this cross-section. When no roll minimum existed (see the roll minimum definition in the previous paragraph), the ‘saddle point’ on this cross-section was calculated as the roll minimum defined, because the potential energy increases monotonically along the imaginary route from pitch to roll minimum. On the 1D yaw cross-section, the ‘saddle point’ is actually a local maximum. We refer to them all as saddle points for simplicity.

We then defined the transition barrier as the potential energy increase from the starting minimum to the saddle point. Note that the imaginary route was only for defining the saddle point, and during the transition the animal did not necessarily start from a local

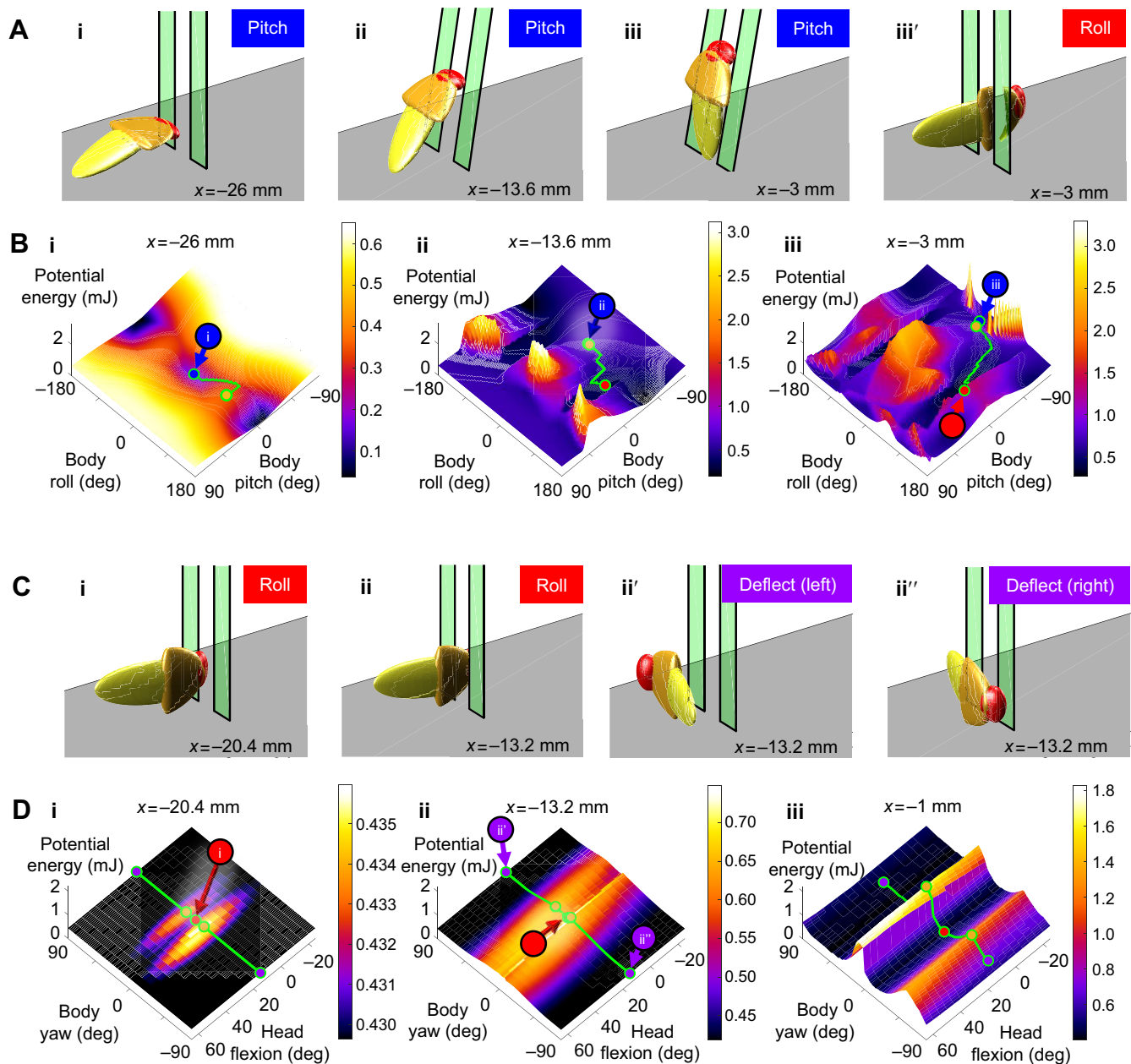


**Fig. 4. Potential energy landscape analyses to quantify transition barriers.** (A,B) Illustration of pitch-roll landscape cross-section analysis to test hypotheses 1 and 2. (C,D) Illustration of yaw landscape cross-section analysis to test hypothesis 3. (A) Illustration of locomotor modes for pitch-roll cross-section. (i) Pitch mode at  $x=-26$  mm (pitch, roll=0 deg, 0 deg). (ii) Pitch mode at  $x=-13.6$  mm (pitch, roll=-38 deg, 0 deg). (iii) Pitch mode at  $x=-3$  mm (pitch, roll=-73 deg, 0 deg). (iii') Roll mode at  $x=-3$  mm (pitch, roll=-8 deg, 92 deg). (B) Pitch-roll landscape cross-section at different  $x$  for quantifying the pitch-to-roll transition barrier. The blue point is the pitch local minimum. The red point is the roll local minimum. The orange point is the saddle point. Green curves are imaginary routes. (i)  $x=-26$  mm. Note that the roll minimum and saddle point overlap here. (ii)  $x=-13.6$  mm. Pitch minimum and saddle point are close. (iii)  $x=0$  mm. (C) Illustration of locomotor modes for yaw cross-section. (i) Roll mode at  $x=-20.4$  mm, yaw=0 deg. (ii) Roll mode at  $x=-13.2$  mm, yaw=0 deg. (ii') Deflect mode at  $x=-13.2$  mm, to the left, yaw=90 deg. (ii'') Deflect mode at  $x=-13.2$  mm, to the right, yaw=-90 deg. (D) Yaw landscape cross-sections stacked along head flexion dimension at different  $x$  for quantifying the roll-to-deflect transition barrier. The red point is the roll local minimum. Purple points are deflect local minima, with positive yaw deflected to the left and negative yaw to the right. Orange points are saddle points. Green curves are imaginary routes. Only routes at head flexion  $\beta_h=15$  deg are marked. (i)  $x=-20.4$  mm. (ii)  $x=-13.2$  mm. (iii)  $x=-1$  mm. In B and D, i, ii, ii', iii and iii' in circles refer to locomotor modes in A and C. Note that the imaginary route is only for defining the saddle point, and during the transition the animal did not necessarily start from a local minimum or transition by crossing the saddle point. In B, body  $y$  and yaw at each  $x$  follow those of the average trajectory (see Materials and Methods, 'Potential energy landscape generation'; Fig. S2). In D, body  $y$ , pitch and roll at each  $x$  follow those of the average trajectory (see Materials and Methods, 'Potential energy landscape generation'; Fig. S2). In both B and D, head flexion is fixed at 15 deg, and abdomen flexion is fixed at 7 deg. In all illustrations and landscapes shown here, legs are neglected; however, legs were modeled when testing hypothesis 2 (see Materials and Methods, 'Testing the usefulness of leg tucking in'; Fig. 10B; Fig. S1B). Also see Movie 3 for an illustration of how the landscapes evolve as a function of  $x$ .

minimum or transition by crossing the saddle point. Despite this, our barrier estimation still provided useful insight as it quantified the level of the difficulty to transition.

Intuitively, the breadth-first search approach resembled injecting water slowly at the start minimum and tracking the expansion of the water-covering area. The potential energy landscape resembled an

uneven surface (Fig. S4A), and each basin on the surface corresponded to a locomotor mode, such as pitch and roll modes (Othayoth et al., 2020) (Fig. S4A, blue and red points; Fig. S4B, blue and red area, separately). Increasing the cost resembled injecting water in the starting basin (Fig. S4B, blue area) and increasing the water level. As the water level increased, there was a moment that the water level was sufficiently high to overcome a barrier between two basins (Fig. S4B, the boundary between blue and red areas), and the water flowed via the saddle point of the barrier (Fig. S4B, orange point) into the destination basin. The water level measured from the starting minimum at the time of this onset of flow resembled the potential energy barrier height (Fig. S4C, yellow).

### Testing the usefulness of head flexion

To test hypothesis 1, we analyzed whether head flexion in the range observed reduced the pitch-to-roll transition barrier compared with if the animal simply held its head in the typical orientation (average head flexion during running on flat ground). We varied head flexion within  $[-25 \text{ deg}, 65 \text{ deg}]$  (covering the observed head flexion range of  $[-24 \text{ deg}, 64 \text{ deg}]$  over all the trials) with an increment of 5 deg (Fig. S1A), calculated the pitch-to-roll transition barrier as a function of  $x$ , and compared the transition barrier at each head flexion with that at head flexion  $\beta_h=15 \text{ deg}$ , which represents the case without active head flexion (temporal average of head flexion was  $\beta_h=15\pm 4 \text{ deg}$  in the approach phase over all trials).

To test hypothesis 3, we analyzed whether the head flexion in the range observed increased the roll-to-deflect transition barrier compared with that without active head flexion. We varied the head flexion as above, calculated the roll-to-deflect transition barrier as a function of  $x$ , and compared the transition barrier at each head flexion with that at head flexion  $\beta_h=15 \text{ deg}$ .

### Testing the usefulness of leg tucking in

To test hypothesis 2, we analyzed whether the leg sprawl changes affected the pitch-to-roll transition barrier. We added two hindlegs (length 27 mm; see ‘Potential energy landscape model definition’, above) into the model symmetrically to the left and right sides of the body, with a leg height of  $-5 \text{ mm}$  (temporal average of leg height was  $-5\pm 3 \text{ mm}$  in the explore+pitch phase over all trials; see Results, ‘Leg adjustments’), and varied total leg sprawl within  $[0 \text{ deg}, 180 \text{ deg}]$  with an increment of 45 deg (Fig. S1B). We compared the transition barrier at each total leg sprawl with that at total leg sprawl

$\phi_T=160 \text{ deg}$  (mean $\pm$ s.d. of maximal total leg sprawl was  $\phi_T=156\pm 21 \text{ deg}$  in the explore+pitch phase over all trials) and  $\phi_T=20 \text{ deg}$  (mean $\pm$ s.d. of minimal total leg sprawl was  $\phi_T=21\pm 17 \text{ deg}$  in the roll phase over all trials). Note that the animal also elevated and depressed its hindlegs asymmetrically in pitch and roll phases (see Results, ‘Leg adjustments’). For simplicity, here we kept the two legs symmetrical to provide a rough estimate of the effect of leg sprawl change on the barrier.

Frequently used averaged variables in landscape analyses are summarized in Table S2.

## RESULTS

### Similar overall performance and behavior to previous study

The animals displayed a similar locomotor performance to that in the previous study (Othayoth et al., 2020), with a similar traversal time ( $3.0\pm 1.0 \text{ s}$  versus  $3.9\pm 3.9 \text{ s}$  previously,  $P=0.18$ , fixed-effects ANOVA). The animal also always transitioned to the roll mode to traverse (100% of all 36 trials), similar to the previous study (97% of all previous trials for slightly less stiff beams  $K=1.7 \text{ mN m rad}^{-1}$ ), with a similar maximal body roll during traversal ( $81\pm 10 \text{ deg}$  versus  $84\pm 20 \text{ deg}$  previously,  $P=0.30$ , fixed-effects ANOVA). Note that even counting the 28 trials not included in the dataset (see Materials and Methods, ‘Experiment protocol’), which had a slightly longer duration, these metrics were still similar (traversal time:  $4.5\pm 1.8 \text{ s}$  versus  $3.9\pm 3.9 \text{ s}$ ,  $P=0.71$ , fixed-effects ANOVA; roll mode use: 98% versus 97% of all trials; maximal body roll:  $90\pm 20 \text{ deg}$  versus  $84\pm 20 \text{ deg}$ ,  $P=0.09$ , fixed-effects ANOVA).

### Cockroaches use complex motion to transition from pitch to roll mode

After running with an alternating tripod gait and colliding with the beams (approach phase; Fig. 5, green), the animal traversed the beam obstacles with complex body, head and leg motions. In the explore+pitch phase (Fig. 5, blue), the animal often moved along the beam layer ( $y$ -direction) and turned left or right to search around the beams, pitched up its body against the beams, repeatedly flexed its head, and rubbed its pronotum against the beams, sometimes pushing the beam using its forelegs or middle legs, and swept its antennae in the gaps. In the roll phase (Fig. 5, red), the animal rolled its body into the gap and struggled with its legs to try to push against the back side of the beams. It sometimes flexed its head repeatedly. It also sometimes flexed and twisted its abdomen.

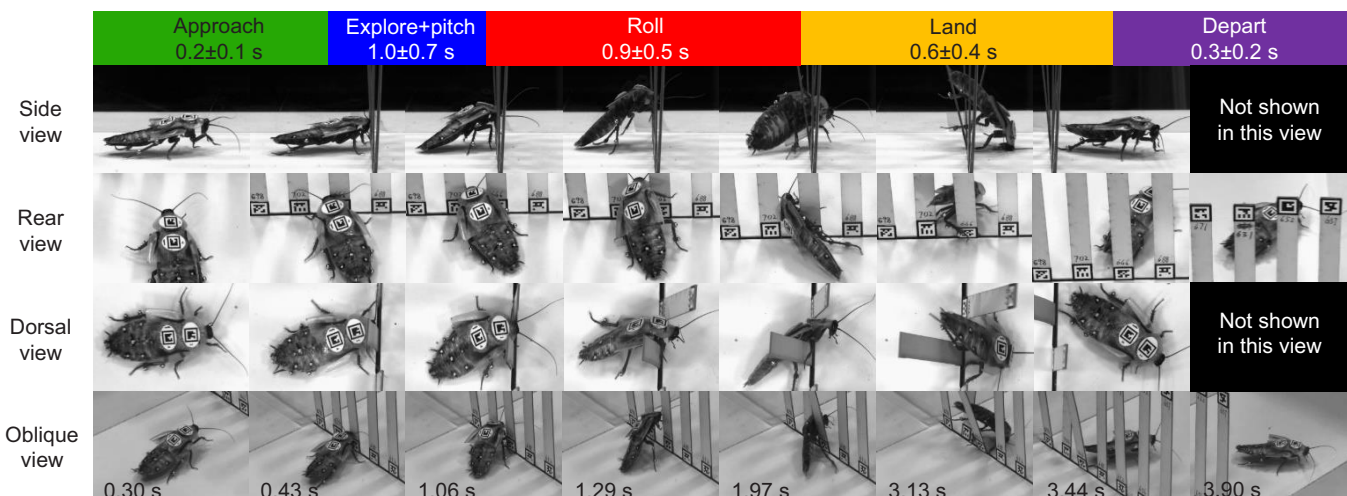


Fig. 5. The five phases of traversal. Values under phase labels are means $\pm$ s.d. of the duration of each phase across all trials.

In the land phase (Fig. 5, orange), the animal continued to do these, eventually passed the beams in the roll mode, and resumed an upright body orientation. Finally, in the depart phase (Fig. 5, purple), the animal ran away in an alternating-tripod gait. These observations were consistent with those in our previous study (Othayoth et al., 2020).

Similar to the previous study, body oscillation was observed (Othayoth et al., 2020). The average kinetic energy fluctuation was  $0.01 \pm 0.01$  mJ. This was smaller than that in the previous study ( $0.02 \pm 0.01$  mJ). We speculate that this was caused by the additional modifications on the animal (wing trimming, adding one more tag on the pronotum, and beads on hindlegs) that slightly resisted animal motion.

### Body rotations

The animal's body pitched up in the explore+pitch phase and rolled into the gap in the roll phase (Fig. 6A; Movie 1). In the approach phase, the body only slightly pitched up (Fig. 6Av,D, green, average pitch  $\beta = -8 \pm 7$  deg; note that a negative body pitch angle means the body pitched up). In the explore+pitch phase, the body pitched up

substantially (pitch angle became more negative, minimal pitch  $\beta = -36 \pm 9$  deg; Fig. 6Aii,vi,D, blue). In the roll phase, as the animal rolled its pitched-up body substantially into the gap (maximal roll  $\gamma = 81 \pm 10$  deg; Fig. 6Aiii,vii,B, red), the body became less pitched (pitch angle less negative; Fig. 6Aiii,vii,D, red) and eventually horizontal. Average body roll  $\gamma$  was higher in the roll phase ( $44 \pm 8$  deg) than in the approach ( $-2 \pm 3$  deg), explore+pitch ( $-3 \pm 6$  deg), and depart ( $-2 \pm 4$  deg) phases (Fig. 6C,  $P < 0.0001$ , repeated-measures ANOVA). Average body pitch  $\beta$  was lower (meaning the body was more pitched up) in the explore+pitch ( $-14 \pm 9$  deg) and roll ( $-14 \pm 9$  deg) phases than in the approach ( $-8 \pm 7$  deg) and depart ( $-7 \pm 5$  deg) phases (Fig. 6E,  $P < 0.05$ , repeated-measures ANOVA).

### Head flexion

During both the explore+pitch and roll phases, the animal sometimes repeatedly flexed its head dynamically and sometimes flexed its head down and held it statically (Fig. 7Ai,iii,B, blue and red; Movie 1). This motion was absent during the approach and depart phases when the animal ran on flat ground (Fig. 7Ai,iv,B,

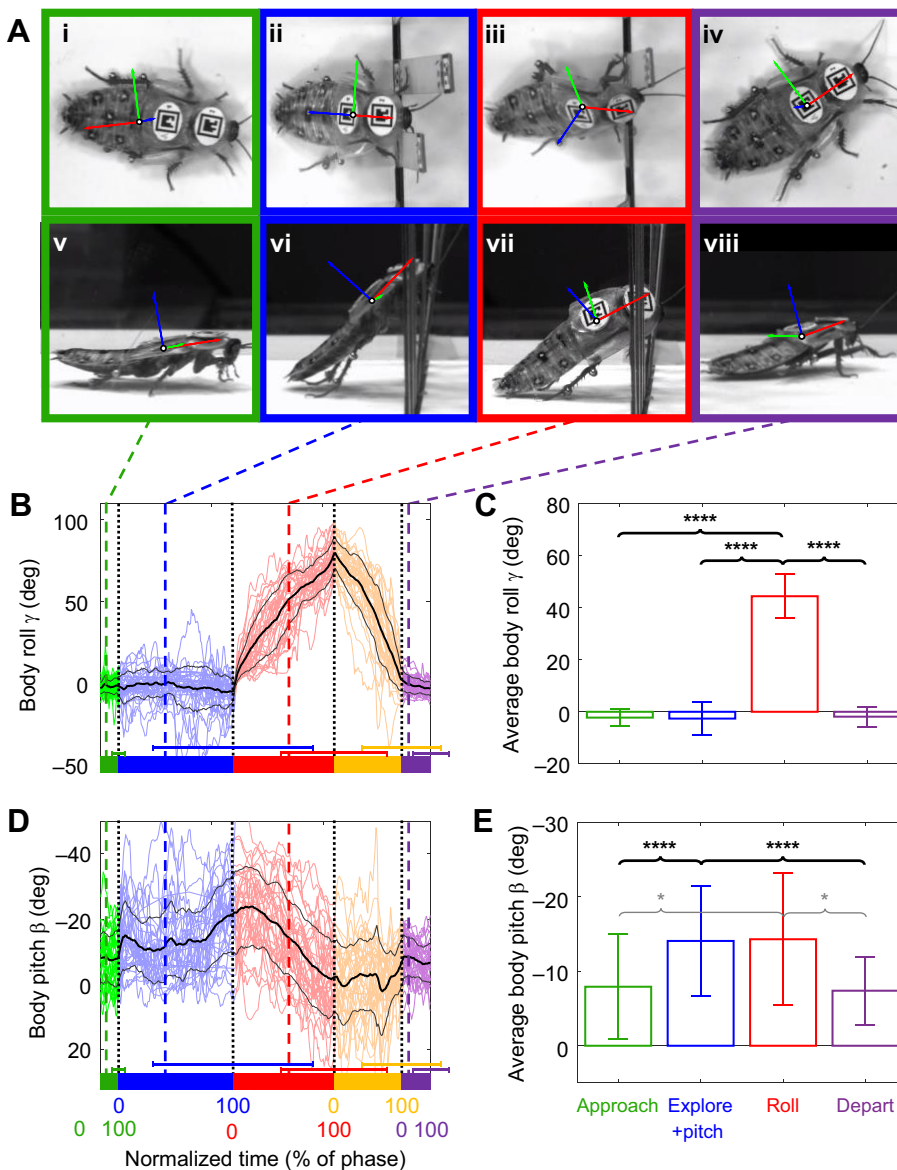


**Fig. 6. Body rotations.** (A) Representative snapshots for each phase. Top and bottom rows show thorax frame from top and side view in approach (i,v), explore+pitch (ii,vi), roll (iii,vii) and depart (iv,viii) phases. The animal's body orientation is represented by Euler angles of thorax frame (yaw  $\alpha$ , pitch  $\beta$ , roll  $\gamma$ , Z–Y–X" Tait–Bryan convention, see Materials and Methods, 'Kinematics and kinetic energy fluctuation analyses'). For simplicity, we laterally mirrored kinematic data of the trials in which the animal rolled to the left to become rolling to the right to simplify the analysis, considering lateral symmetry (see Materials and Methods, 'Kinematics and kinetic energy fluctuation analyses'). (B,D) Body roll (B) and pitch (D) as a function of time, with time of each phase offset to zero at its beginning and then normalized to its duration to be percentage of each phase (see Materials and Methods, 'Statistics'). Colors are for the five phases defined in Fig. 5. The length of the horizontal colored thick bars and the error bars are proportional to means  $\pm$  s.d. of the duration of each phase of all trials shown in Fig. 5. Black vertical dotted lines separate consecutive phases. Colored dashed lines show moments of snapshots in A. Colored curves are individual trials. Thick and thin black curves are mean  $\pm$  s.d. across all trials. (C,E) Average body roll and pitch in different phases. Bars and error bars are means  $\pm$  s.d. of the temporal averages of all trials in B and D for each phase. \* $P < 0.05$ , \*\*\*\* $P < 0.0001$ , repeated-measures ANOVA. Bold brackets and asterisks show important comparisons described in the Results. In D and E, the y-axis is inverted to better show body pitching up more or less, because a negative body pitch angle means the body is pitched up.

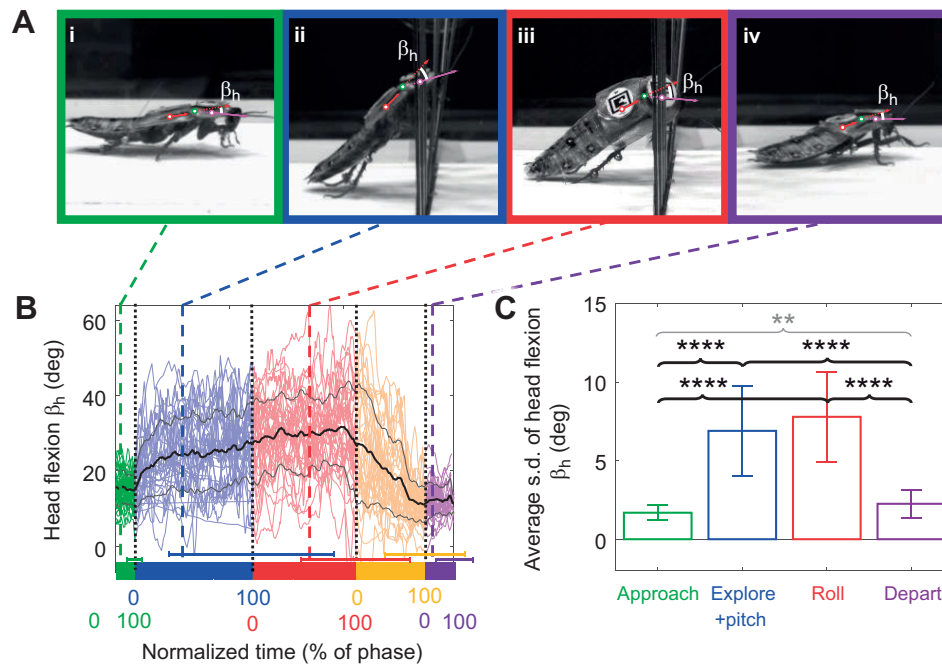


**Fig. 7. Head flexion.** (A) Representative snapshots for each phase. The four panels show head flexion  $\beta_h$  (defined as pitch angle of the head in thorax frame; see Materials and Methods, ‘Kinematics and kinetic energy fluctuation analyses’) in approach (i), explore+pitch (ii), roll (iii) and depart (iv) phases. For simplicity, we laterally mirrored kinematic data of the trials in which the animal rolled to the left to become rolling to the right to simplify the analysis, considering lateral symmetry (see Materials and Methods, ‘Kinematics and kinetic energy fluctuation analyses’). (B) Head flexion as a function of time, with time of each phase offset to zero at its beginning and then normalized to its duration to be percentage of each phase (see Materials and Methods, ‘Statistics’). Colors are for the five phases defined in Fig. 5. The length of the horizontal colored thick bars and the error bars are proportional to mean  $\pm$  s.d. of the duration of each phase of all trials shown in Fig. 5. Black vertical dotted lines separate consecutive phases. Colored dashed lines show moments of snapshots in A. Colored curves are individual trials. Thick and thin black curves are mean  $\pm$  s.d. across all trials. (C) Average standard deviation of head flexion in different phases. Bars and error bars are mean  $\pm$  s.d. of the temporal standard deviations of all trials in B for each phase. \*\* $P < 0.01$ , \*\*\*\* $P < 0.0001$ , repeated-measures ANOVA. Bold brackets and asterisks show important comparisons described in the Results.

green and purple). The standard deviation of the head flexion  $\beta_h$ , which reflects how much the head flexed (see Materials and Methods, ‘Kinematics and kinetic energy fluctuation analyses’), was higher in the explore+pitch ( $7 \pm 3$  deg) and roll ( $8 \pm 3$  deg) phases than in the approach ( $1.7 \pm 0.5$  deg) and depart ( $2 \pm 1$  deg) phases (Fig. 7C,  $P < 0.0001$ , repeated-measures ANOVA).

### Abdomen flexion

During both the explore+pitch and roll phases, the animal sometimes repeatedly flexed its abdomen dynamically and sometimes flexed its abdomen down and held it statically (Fig. 8Aii,iii,B, blue and red; Movie 1). This motion was absent during the approach and depart phases when the animal ran on flat ground (Fig. 8Ai,iv,B, green and purple). The standard deviation of the abdomen flexion  $\beta_a$ , which reflects how much the abdomen flexed (see Materials and Methods, ‘Kinematics and kinetic energy fluctuation analyses’), was higher in the roll ( $7 \pm 3$  deg) and explore+pitch ( $4 \pm 2$  deg) phases than in the approach ( $2 \pm 1$  deg) and depart ( $3 \pm 1$  deg) phases (Fig. 8C,  $P < 0.0001$ , repeated-measures ANOVA).

### Leg adjustments

The animal adjusted its hindlegs in two ways (Fig. 9A; Movie 2). First, it adjusted its hindleg sprawl in the explore+pitch and roll phases. During the explore+pitch phase, the animal spread both its hindlegs further outward (Fig. 9Aii) compared with the approach phase (Fig. 9Ai,B; average left leg sprawl angle  $\phi_L = 63 \pm 15$  deg versus  $55 \pm 10$  deg, average right leg sprawl angle  $\phi_R = 64 \pm 13$  deg versus  $55 \pm 11$  deg). As body rolling began, the animal tucked in its

depressed (left) hindleg (Fig. 9Aiii,B, blue; average left leg sprawl angle  $\phi_L = 27 \pm 21$  deg) while keeping the right leg sprawl relatively unchanged (Fig. 9Aiii,B, red; average right leg sprawl angle  $\phi_R = 62 \pm 13$  deg). Average total leg sprawl  $\phi_T$  was greater in the explore+pitch phase ( $\phi_T = 127 \pm 19$  deg) and smaller in the roll phase ( $90 \pm 23$  deg) than in the approach ( $110 \pm 13$  deg) and depart ( $115 \pm 11$  deg) phases (Fig. 9C,  $P < 0.0001$ , repeated-measures ANOVA).

In addition, the animal depressed one hindleg relative to the body and elevated the other in the roll phase. In the explore+pitch phase, the two hindlegs had similar heights (Fig. 9Avi,vi',D; average left leg height  $h_L = -4 \pm 2$  mm, average right leg height  $h_R = -5 \pm 2$  mm, average leg height difference  $\Delta h = -1 \pm 2$  mm). In the roll phase, the animal usually kept both feet on the ground (Fig. 9Avii,vii'), with one hindleg depressed further (Fig. 9D, blue; average leg heights  $h_L = -11 \pm 3$  mm), appearing to push against the ground (Fig. 9Avii,vii'), while the other elevated (Fig. 9D, red; average leg heights  $h_R = -2 \pm 2$  mm), appearing to support the body (Fig. 9Avii,vii'), which increased the leg height difference (Fig. 9E, red). As the animal moved further through the gap and reached maximal body roll, it elevated its depressed (left) leg up to around the body coronal plane (maximal leg height  $h_L = 4 \pm 3$  mm) in the land phase (Fig. 9D, blue). The average leg height difference  $\Delta h$  was higher in the roll phase ( $9 \pm 3$  mm) than in the approach ( $-1 \pm 1$  mm), explore+pitch ( $-1 \pm 2$  mm) and depart ( $-1 \pm 1$  mm) phases (Fig. 9E,  $P < 0.0001$ , repeated-measures ANOVA). Both these observations demonstrated that the animal used its left and right hindlegs differentially in the roll phase.

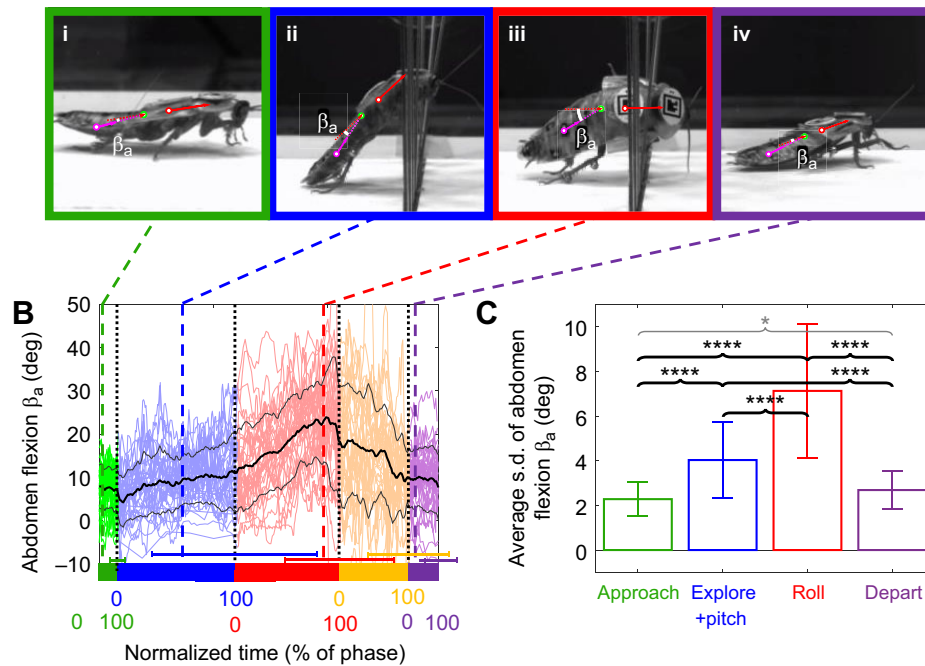


**Fig. 8. Abdomen flexion.** (A) Representative snapshots for each phase. The four panels show abdomen flexion  $\beta_a$  (defined as pitch angle of the abdomen in thorax frame; see Materials and Methods, ‘Kinematics and kinetic energy fluctuation analyses’) in approach (i), explore+pitch (ii), roll (iii) and depart (iv) phases. For simplicity, we laterally mirrored kinematic data of the trials in which the animal rolled to the left to become rolling to the right to simplify the analysis, considering lateral symmetry (see Materials and Methods, ‘Kinematics and kinetic energy fluctuation analyses’). (B) Abdomen flexion as a function of time, with time of each phase offset to zero at its beginning and then normalized to its duration to be percentage of each phase (see Materials and Methods, ‘Statistics’). Colors are for the five phases defined in Fig. 5. The length of the horizontal colored thick bars and the error bars are proportional to means $\pm$ s.d. of the duration of each phase of all trials shown in Fig. 5. Black vertical dotted lines separate consecutive phases. Colored dashed lines show moments of snapshots in A. Colored curves are individual trials. Thick and thin black curves are mean $\pm$ s.d. across all trials. (C) Average abdomen flexion angle in different phases. Bars and error bars are means $\pm$ s.d. of the temporal standard deviations of all trials in B for each phase. \* $P$ <0.05, \*\*\*\* $P$ <0.0001, repeated-measures ANOVA. Bold brackets and asterisks show important comparisons described in the Results.

### Refined potential energy landscape is consistent with coarse landscape in previous study

The topology and evolution of the refined potential energy landscape (Movie 3) as viewed in the pitch–roll cross-section were consistent with those in our previous study (Othayoth et al., 2020). Initially, when the animal was far from the beam, the energy landscape had a local minimum at zero pitch and roll, and a basin was formed near the minimum; as the body moved close to the beam, the basin moved along the pitch direction, becoming the pitch basin, while the roll basin formed at about zero pitch and about 90 deg roll. The similarity of the topology of the potential energy landscape indicated that it was insensitive to minor differences in shape modeling (e.g. using refined body shape versus using a simple ellipsoidal body; varying head and abdomen flexion; including hindlegs or not). We also found that the pitch-to-roll transition barrier calculated from the refined potential energy landscape model here is similar to that from the simple model in the previous study (see Supplementary Materials and Methods, ‘Pitch-to-roll transition barrier’), further demonstrating the model’s consistency and applicability with both coarse-grained and fine-grained model approximations (see discussion in Othayoth et al., 2020).

Because we allowed the beam to deflect backward, the pitch basin finally went back to near-zero pitch, and the roll basin eventually disappeared. The landscape became the initial landscape as the animal had traversed and moved far from the beam. This showed that the beam deflection calculation was more reasonable than in the previous study.

### Head flexion does not facilitate the pitch-to-roll transition

To test hypothesis 1 that active head flexion reduces the pitch-to-roll transition barrier and facilitates rolling into the gap, we analyzed whether adjusting head flexion can reduce the pitch-to-roll transition barrier. The transition barrier from the pitch to the roll mode with different head flexion is shown in Fig. 10A. At the average  $x$  (−13.6 mm) where the animals transitioned from pitch to roll mode, the maximal transition barrier reduction with head flexion within [−25 deg, 65 deg] was 0.0027 mJ (Fig. 10A, a). This mechanical energy that could be saved by head flexion was small (27%) compared with the average kinetic energy fluctuation level (0.01 mJ) and small (4.5%) compared with the energy saved by leg tucking in (0.06 mJ; see ‘Leg sprawl adjustments facilitate body rolling’, below). Also, achieving this saving would require the head to flex by 65 deg, which was rarely observed in the experiment. This suggested that the head adjustment did not reduce the transition barrier substantially to facilitate the pitch-to-roll transition. This rejected our hypothesis that the head adjustment facilitated the mode transition by lowering the pitch-to-roll transition barrier on the potential energy landscape.

To test hypothesis 3 that active head flexion facilitates the animal staying within the gap after rolling into it, we analyzed whether adjusting head flexion can increase the roll-to-deflect transition barrier. The transition barrier from the roll to the deflect mode with different head flexion is shown in Fig. 10C,D. At the average  $x$  (−13.6 mm) where the animal transitioned from the pitch to the roll mode, the maximal increase in the transition barrier with head flexion within [−25 deg, 65 deg] was 0.012 mJ (Fig. 10C, c) to

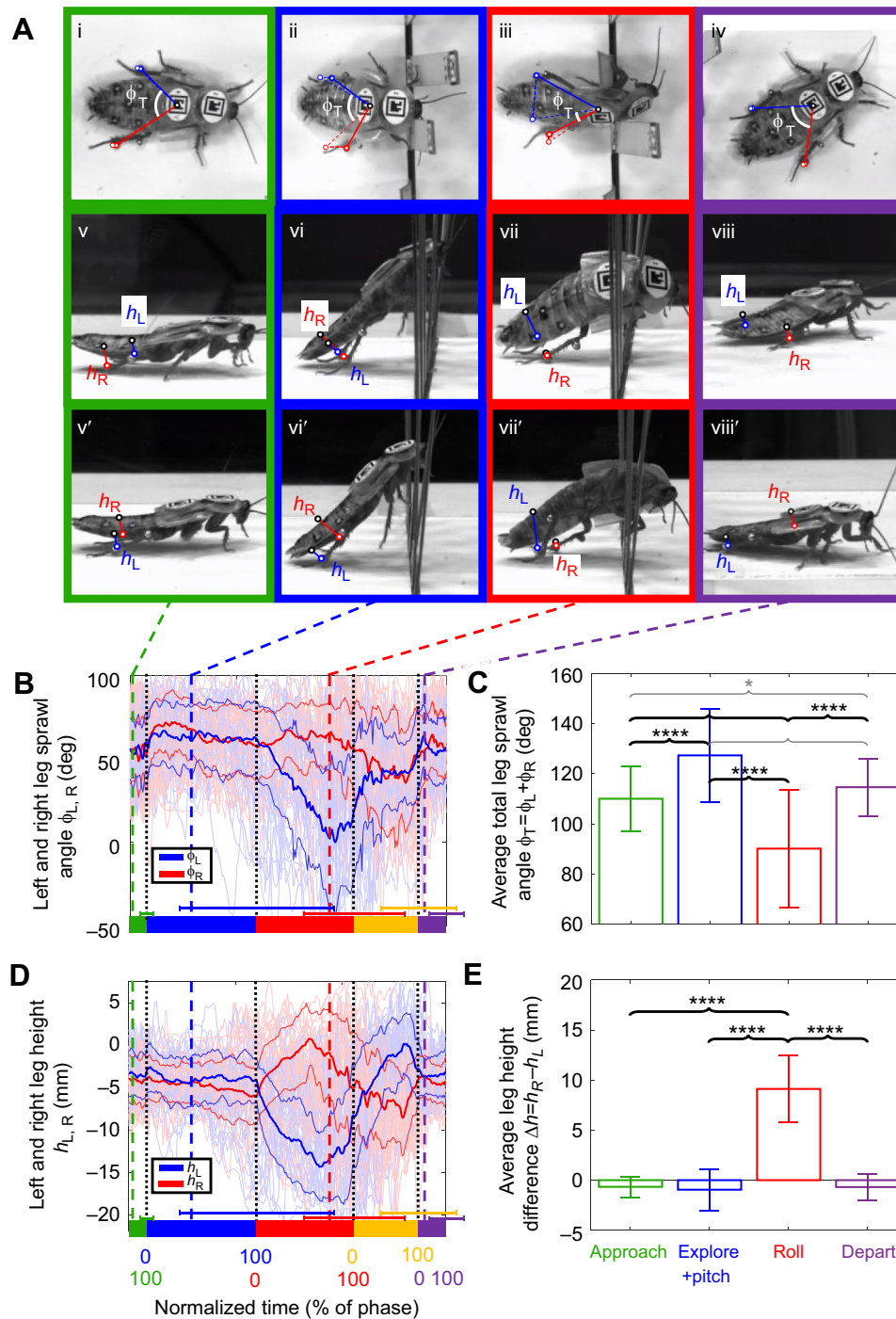


**Fig. 9. Leg adjustments.** (A) Representative snapshots for each phase. Top row shows total leg sprawl  $\phi_T$  (defined as the angle between two leg vectors in body coronal plane; see Materials and Methods, 'Kinematics and kinetic energy fluctuation analyses') in approach (i), explore+pitch (ii), roll (iii) and depart (iv) phases. Middle row shows left leg height  $h_L$  (blue) and right leg height  $h_R$  (red) (defined as leg distance to body coronal plane; see Materials and Methods, 'Kinematics and kinetic energy fluctuation analyses') in approach (v), explore+pitch (vi), roll (vii) and depart (viii) phases, respectively. For simplicity, we laterally mirrored kinematic data of the trials in which the animal rolled to the left to become rolling to the right to simplify the analysis, considering lateral symmetry (see Materials and Methods, 'Kinematics and kinetic energy fluctuation analyses'). Bottom row (v',vi',vii',viii') shows mirrored lateral views from cameras opposite to the middle row ones (v,vi,vii,viii) to better show legs on the opposite side. (B,D) Leg sprawl angle and leg height of hindlegs as a function of time, with time of each phase offset to zero at its beginning and then normalized to its duration to be percentage of each phase (see Materials and Methods, 'Kinematics and kinetic energy fluctuation analyses'). A negative leg height means that the leg marker is below body coronal plane, and a positive leg height means the leg marker is above it. The length of the horizontal colored thick bars and the error bars are proportional to means  $\pm$  s.d. of the duration of each phase of all trials shown in Fig. 5, the colors of which correspond to the five phases defined in Fig. 5. Black vertical dotted lines separate consecutive phases. Colored dashed lines show moments of snapshots in A. Light-colored curves are individual trials. Thick and thin dark-colored curves are mean  $\pm$  s.d. across all trials. Blue and red colors are for left and right legs, respectively. (C,E) Average total leg sprawl and leg height in different phases. Bars and error bars are means  $\pm$  s.d. of the temporal averages of all trials in B and D for each phase. \* $P < 0.05$ , \*\*\*\* $P < 0.0001$ , repeated-measures ANOVA. Bold brackets and asterisks show important comparisons described in the Results.

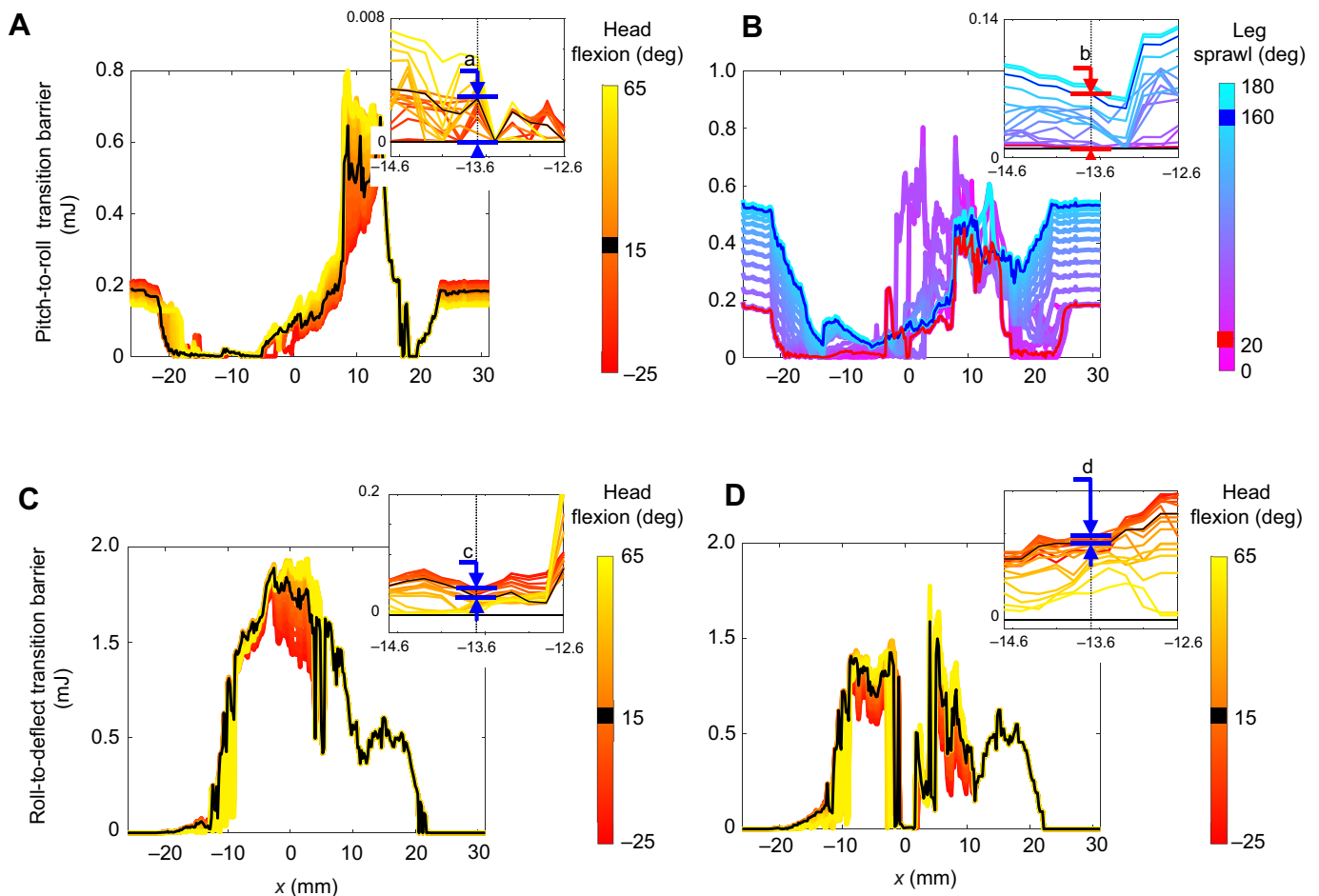


**Fig. 10. Effect of head flexion and leg sprawl on transition barriers.** (A,B) Pitch-to-roll transition barrier as a function of  $x$  for different head flexion (A) and total leg sprawl (B). (C,D) Roll-to-deflect transition barrier as a function of  $x$  for different head flexion to the left (C) and right (D). In A, C and D, black curves show the transition barrier at average animal head flexion  $\beta_h = 15$  deg. In B, red and blue curves show the transition barrier at total leg sprawl  $\phi_T = 20$  deg and 160 deg, respectively. Insets in A–D are close-up views in the  $x$  range of  $[-14.6$  mm,  $-12.6$  mm], respectively. Dashed lines show  $x = -13.6$  mm, which is the average location when roll phase begins. a–d show the maximal transition barrier increase or reduction by using active adjustments. See Movie 3 for an illustration of how barrier as a function of  $x$  is obtained. In A and B, body  $y$  and yaw at each  $x$  follow those of the average trajectory (see Materials and Methods, ‘Potential energy landscape generation’; Fig. S2). In C and D,  $y$ , pitch and roll at each  $x$  follow those of the average trajectory (see Materials and Methods, ‘Potential energy landscape generation’; Fig. S2). In A, C and D, hindlegs are neglected, and the abdomen is flexed at 7 deg. In B, head flexion is fixed at 15 deg, and abdomen flexion is fixed at 7 deg.

deflect to the left and 0.008 mJ (Fig. 10D, d) to deflect to the right. The transition barrier only increased by a maximum of 12%, which required the head to hyperextend (head flexion  $\beta_h = -25$  deg), which was rarely observed in the experiment. This suggested that the head adjustment did not increase the transition barrier substantially to prevent the animal from yawing to deflect the beams. This rejected our hypothesis that the head adjustment facilitates the body staying within the gap.

### Leg sprawl adjustments facilitate body rolling

To test hypothesis 2 that tucking in a hindleg reduces the pitch-to-roll transition barrier and facilitates rolling, we analyzed how adjusting leg sprawl changes the pitch-to-roll transition barrier. The transition barrier from pitch to roll mode with different total leg sprawl is shown in Fig. 10B. At  $x = -13.6$  mm, where the animals transitioned from the pitch to roll mode, the transition barrier at 20 deg total leg sprawl was less than that at 160 deg total leg sprawl by 0.06 mJ (Fig. 10B, b), which is 6 times larger than the average kinetic energy fluctuation level. This indicates that tucking a hindleg in helped the animal substantially reduce the pitch-to-roll

transition barrier when rolling. Together, these findings supported our hypothesis that leg sprawl adjustment facilitated the pitch-to-roll transition.

Curiously, at  $x = -20$  mm, where the animals pitched against the beams (temporal average of  $x$  was  $-20 \pm 3$  mm in the pitch+explore phase over all trials), the transition barrier at 160 deg total leg sprawl was larger than that at 20 deg total leg sprawl by 0.35 mJ, which was 35 times larger than the animal’s average kinetic energy fluctuation (0.01 mJ). Because a larger potential energy barrier indicates higher stability, this suggests that further spreading out the hindlegs during the pitch+explore phase helped the animal stay pitched up against the beams more stably and resist rolling into the gap. We speculate that in this phase the larger leg spread here helped the animal’s pitched-up body stay aligned to the gap rather than yaw and fall sideways under gravity.

### DISCUSSION

As a first step to understand how animals actively control their physical interaction with complex 3D terrain to transition between locomotor modes, we quantified active adjustments by the discoid

cockroach to make the pitch-to-roll transition while traversing beam obstacles. The major adjustments included body rotations (Fig. 6), head flexion (Fig. 7), abdomen flexion (Fig. 8) and differential hindleg use (Fig. 9). Because it was strenuous to traverse the stiff beams by pushing across (the pitch mode), the animal likely made these active adjustments to facilitate transitioning to the less strenuous roll mode. Below, we discuss the likely function of each adjustment and suggest future directions.

### Role of head flexion

To find the function of active head flexion in both the explore+pitch and roll phases, we first hypothesized that by changing the overall body shape, it (1) lowered the pitch-to-roll transition barrier and (2) increased the roll-to-deflect transition barrier. However, we found that head flexion did not change the transition barrier substantially in both cases. Therefore, we rejected these two hypotheses (see Results, 'Head flexion does not facilitate the pitch-to-roll transition'). We speculate that this is because the cockroach's head is small and relatively more spherical (thickness/length=0.66) compared with the thorax (thickness/length=0.30) and abdomen (thickness/length=0.21), so its orientation does not change overall body shape substantially, resulting in too small a change in the potential energy landscape.

We speculate that the animal flexed its head to sense obstacle properties in the explore+pitch phase. Groups of campaniform sensilla and sensory hairs embedded in the cockroach's pronotum can sense the magnitude, direction and position of the terrain reaction force (Delcomyn et al., 1996). The chordotonal organ in the animal's neck can detect the forces pushing against the head (Field and Matheson, 1998; Tuthill and Wilson, 2016). These could help the animal estimate the obstacle's physical properties (stiffness, surface friction coefficient, etc.) (Xuan et al., 2022 preprint) and guide its active adjustments to better traverse. We speculate that the occasional dynamically changing head flexion is a form of active tactile sensing (Mongeau et al., 2013; Prescott et al., 2011; Staudacher et al., 2005). We observed that the animal seemed to hyperextend the head upward in order to find the top end of the stiff beam obstacles (to initiate climbing) and flexed the head downward in order to find a gap to move into.

In addition, we speculate that the animal flexed its head in the land phase (after the center of mass had passed the beams) to help its forelegs reach the ground to help propel it forward, while its middle legs and hindlegs were still interacting with the beams and were likely less effective at generating propulsion within the narrow gap. This is similar to cockroaches flexing the head to help the forelegs reach the top surface when climbing a large step (Ritzmann et al., 2005).

Although head flexion is not driven by the same muscle group as abdomen flexion or hindleg movement (Sanderson and Jackson, 1912), it is possible that it can be indirectly triggered by the abdomen motion (e.g. via sensory feedback for coordination). Further analysis of the correlation between adjustments will test these possibilities.

### Role of abdomen flexion

We speculate that the animal flexed its abdomen frequently in the roll and land phases to generate kinetic energy fluctuation to break resistive frictional and interlocking contact as it pushed through the beams when the body had rolled into the gap. Because the beam gap was narrow and barely larger than the animal body thickness (average body thickness not including legs was only 73% of gap width), the animal had to elevate its legs closer to the body to fit them within the gap. This made it difficult to generate thrust force

from the legs. Meanwhile, the spines and other asperities on the thorax, abdomen and legs added resistance, similar to a cockroach crawling in a confined space (Jayaram and Full, 2016). This kinetic energy fluctuation from abdomen flexion helps the animal become unstuck and facilitates traversal (i.e. likely overcoming very small barriers on a very fine-grained potential energy landscape, if one considers the effects of these small features; see discussion in Othayoth et al., 2020).

### Role of leg adjustments

We speculate that the animal spread its hindlegs further outward to stabilize the pitched-up body against the beams in the pitch+explore phase and tucked in the depressed hindleg (the left one during body rolling to the right) to destabilize it to roll in the roll phase. Geometrically, the stable support polygon of the animal was formed among contacts between its hindfeet and the ground and contacts between its head or thorax and the beams. In the explore+pitch phase, the animal spread its hindlegs out widely, with a large distance between the two hindfeet touching the ground, which increased the animal's roll stability (Fig. S3A). We speculate that this helped the animal's pitched-up body stay aligned to the gap rather than yaw and fall sideways under gravity. In the roll phase, as the animal tucked in its depressed hindleg, the support polygon shrank and the roll margin of stability reduced (Fig. S3B), and the roll stability reduced. These effects can be quantified by the potential energy landscape. The potential energy barrier from the pitch to the roll basin measures the difficulty of the transition. In the explore+pitch phase, further leg spreading increased the transition barrier, which helped the animal stay pitching up against the beams. During the pitch-to-roll transition, tucking in a leg reduced the transition barrier and made rolling easier. We also observed that the animal spread out its elevated hindleg (the right one during body rolling to the right) in the land phase. We speculated that this was to better engage with the ground to propel itself forward when its body was still in the gap.

Aside from leg sprawl, the differential leg uses also played an important role. We speculate that in the beginning of the roll phase the animal depressed one hindleg and elevated the other while keeping both feet on the ground to generate a roll torque. In the land phase, it elevated both hindlegs closer to the body after the body has rolled into the gap, likely to reduce the resistance on the legs from the beams while pushing through.

### Role of body flexibility

Our results further suggest that the flexibility from multiple body parts and articulated leg joints of the entire animal also reduces the efforts of locomotor transition and traversal (Jayaram and Full, 2016; Ritzmann et al., 2005). The animal's body is more flexible and compliant than our rigid body model. This will likely result in a smaller beam flexion than estimated by the model and reduce the transition barrier. The soft, segmented exoskeleton structure also likely reduced interlocking and frictional resistance and facilitated traversal.

### Likely involvement of sensory feedback control

Studies on insects negotiating large obstacles have revealed that the changes in kinematics are often modulated by sensory inputs. For example, when climbing large stairs, stick insects switch from using long to short steps when they have sensed a lack of substrate engagement (Theunissen and Dürre, 2013); when climbing a large step, cockroaches flex the head to help the forelegs reach the top step surface when its head has sensed that it has risen above the step (Ritzmann et al., 2005). During traversal of cluttered beams in our

study, the cockroach's active adjustment to make the pitch-to-roll transition, which was absent when running on a flat ground, was almost certainly driven by sensory input of its environment interaction. During traversal, it took the animal an average time of  $1.3 \pm 0.7$  s to explore and pitch up against the beams before rolling occurred. This is well above the  $\sim 100$  ms that cockroaches need to complete a feedback control loop [6–40 ms for the sensory delay (Ritzmann et al., 2012) and 47 ms for neuromuscular delay (Sponberg and Full, 2008)]. We posit that the animal sensed the terrain and used this information to determine that pushing across was too strenuous and to guide transitioning to the less strenuous roll mode. We have recently explored the feasibility of this strategy in a simple simulated robotic physical model (Xuan et al., 2022 preprint).

### Future work

Future work should test the speculated mechanisms of how each kind of adjustment facilitates the observed locomotor transition. (1) To understand whether and how flexing the head facilitates terrain sensing and how to take advantage of this, we can build a robot with head flexion and force sensing (Wang et al., 2021) and study it systematically with and without feedback control using the sensed forces. (2) To understand whether and how abdomen flexion helps the animal become unstuck, we can build a robot with a flexing abdomen (or tail; Mi et al., 2022) to test whether the flexing of the massive lateral part helps in beam traversal. (3) To test whether active leg adjustment indeed generates a roll torque, we can add highly sensitive yet low-cost force sensors (Li et al., 2019a; Wöhrle et al., 2017) to the ground in front of the beams to measure the ground reaction force on each foot.

To further understand the neural mechanisms involved in such cluttered large obstacle traversal, we can measure the animal's sensory neural signals (Mongeau et al., 2015; Ritzmann et al., 2012) and muscle activity (i.e. electromyogram) (Sponberg and Full, 2008; Watson et al., 2002) and alter the motor activation signal to change active adjustments and test their effect on the body dynamics (Sponberg et al., 2011a,b). The first challenge is to identify what sensors are involved in these cluttered adjustments for large obstacle traversal. Like other insects, cockroaches should have many sensors that can obtain information about the terrain (Delcomyn et al., 1996; Harley et al., 2009; Tuthill and Azim, 2018; Tuthill and Wilson, 2016), including: (1) visual observation of the geometry of the terrain; (2) use of exteroceptors such as tactile hairs to sense the position of an object; (3) use of proprioceptors to sense relative position/velocity between joints to infer object position; and (4) use of campaniform sensilla to detect force and torque exerted on exoskeleton and joints. A first step to identify the relevant sensing modalities is to disable some of these sensing sources, such as blinding the eyes (Spirito and Mushrush, 1979) and disabling the campaniform sensilla (Pearson and Iles, 1973), and observe changes in locomotor behavior and performance. Based on animal observations, computational modeling of neural control (such as in Schilling and Cruse, 2020) may be fruitful for understanding feedback principles governing body and appendage adjustments to traverse cluttered large obstacles. In addition, it may be interesting to study whether animals perform active sensing (Krakauer et al., 2017; Mongeau et al., 2013; Moss et al., 2006; Nelson and MacIver, 2006; Okada et al., 2002; Schütz and Dürr, 2011; Stamper et al., 2012) in the less considered modality of contact force sensing.

Our case study illustrates how to use fine-grained potential energy landscape modeling to understand the locomotor–terrain interaction that involves active adjustments of more body and appendage degrees of freedom, which may lead to the discovery of

attractive basins that result in distinct nuanced locomotor modes (see discussion in Othayoth et al., 2020). Given these advancements, the potential energy landscape modeling still does not fully describe system dynamics, as it only addresses conservative forces of the system that can be expressed as gradients of the potential energy landscape. Future work should systematically measure and model non-conservative and random forces and add them to make the modeling approach predictive. These measurements and a predictive potential energy landscape theory capturing dynamics will reveal how the animal generates propulsive forces and torques to overcome resistive ones in order to destabilize itself from undesired modes (basins) of attraction and steer into the desired modes (basins) and how this process can be guided by terrain force sensing (Xuan et al., 2022 preprint).

### Acknowledgements

We thank Yuanfeng Han and Qiyuan Fu for help with imaging setup, Yuanfeng Han and Qihan Xuan for discussion, and Xiao Yu for help with animal care and manually correcting the marker tracking.

### Competing interests

The authors declare no competing or financial interests.

### Author contributions

Conceptualization: C.L.; Methodology: Y.W., R.O., C.L.; Software: Y.W., R.O.; Validation: Y.W., C.L.; Formal analysis: Y.W.; Investigation: Y.W.; Resources: Y.W., R.O., C.L.; Data curation: Y.W.; Writing - original draft: Y.W.; Writing - review & editing: Y.W., R.O., C.L.; Visualization: Y.W.; Supervision: C.L.; Project administration: C.L.; Funding acquisition: C.L.

### Funding

This research was funded by an Arnold & Mabel Beckman Foundation Beckman Young Investigator Award, a Burroughs Wellcome Fund Career Award at the Scientific Interface, and Johns Hopkins University Whiting School of Engineering start-up funds to C.L. Y.W. was partially supported by funds for an undergraduate research internship from the Department of Mechanical Engineering in Tsinghua University. Open Access funding provided by Johns Hopkins University. Deposited in PMC for immediate release.

### Data availability

MATLAB codes and data files are available from GitHub: [https://github.com/TerradynamicsLab/cockroach\\_adjust.git](https://github.com/TerradynamicsLab/cockroach_adjust.git).

### References

- Alexander, R. M. (2002). *Principles of Animal Locomotion*. Princeton University Press.
- Blaesing, B. and Cruse, H. (2004). Stick insect locomotion in a complex environment: climbing over large gaps. *J. Exp. Biol.* **207**, 1273–1286. doi:10.1242/jeb.00888
- Blickhan, R. and Full, R. J. (1993). Similarity in multilegged locomotion: Bouncing like a monopode. *J. Comp. Physiol. A* **173**, 509–517. doi:10.1007/BF00197760
- Bramble, D. M. and Lieberman, D. E. (2004). Endurance running and the evolution of Homo. *Nature* **432**, 345–352. doi:10.1038/nature03052
- Cormen, T. H., Leiserson, C. E., Rivest, R. L. and Stein, C. (2009). *Introduction to Algorithms*, 3rd edn. The MIT Press.
- Crall, J. D., Gravish, N., Mountcastle, A. M. and Combes, S. A. (2015). BEEtag: a low-cost, image-based tracking system for the study of animal behavior and locomotion. *PLoS ONE* **10**, e0136487. doi:10.1371/journal.pone.0136487
- Delcomyn, F., Nelson, M. E. and Cocatre-Zilgien, J. H. (1996). Sense organs of insect legs and the selection of sensors for agile walking robots. *Int. J. Rob. Res.* **15**, 113–127. doi:10.1177/027836499601500201
- Dickinson, M. H., Farley, C. T., Full, R. J., Koehl, M. A. R., Kram, R. and Lehman, S. (2000). How animals move: an integrative view. *Science* **288**, 100–106. doi:10.1126/science.288.5463.100
- Field, L. H. and Matheson, T. (1998). Chordotonal organs of insects. *Adv. Insect Physiol.* **27**, 1–228. doi:10.1016/S0065-2806(08)60013-2
- Gart, S. W. and Li, C. (2018). Body-terrain interaction affects large bump traversal of insects and legged robots. *Bioinspir. Biomim.* **13**, 026005. doi:10.1088/1748-3190/aaa2d0
- Gart, S. W., Yan, C., Othayoth, R., Ren, Z. and Li, C. (2018). Dynamic traversal of large gaps by insects and legged robots reveals a template. *Bioinspir. Biomim.* **13**, 026006. doi:10.1088/1748-3190/aaa2cd

- Han, Y., Othayoth, R., Wang, Y., Hsu, C.-C., de la Tijera Obert, R., Francois, E. and Li, C. (2021). Shape-induced obstacle attraction and repulsion during dynamic locomotion. *Int. J. Rob. Res.* **40**, 939-955. doi:10.1177/0278364921989372
- Harley, C. M., English, B. A. and Ritzmann, R. E. (2009). Characterization of obstacle negotiation behaviors in the cockroach, *Blaberus discoidalis*. *J. Exp. Biol.* **212**, 1463-1476. doi:10.1242/jeb.028381
- Hedrick, T. L. (2008). Software techniques for two- and three-dimensional kinematic measurements of biological and biomimetic systems. *Bioinspir. Biomim.* **3**, 034001. doi:10.1088/1748-3182/3/3/034001
- Ijspeert, A. J. (2008). Central pattern generators for locomotion control in animals and robots: a review. *Neural Netw.* **21**, 642-653. doi:10.1016/j.neunet.2008.03.014
- Jayaram, K. and Full, R. J. (2016). Cockroaches traverse crevices, crawl rapidly in confined spaces, and inspire a soft, legged robot. *Proc. Natl. Acad. Sci. USA* **113**, E950-E957. doi:10.1073/pnas.1514591113
- Jindrich, D. L. and Full, R. J. (2002). Dynamic stabilization of rapid hexapedal locomotion. *J. Exp. Biol.* **205**, 2803-2823. doi:10.1242/jeb.205.18.2803
- Krakauer, J. W., Ghazanfar, A. A., Gomez-Marín, A., MacIver, M. A. and Poeppel, D. (2017). Neuroscience needs behavior: correcting a reductionist bias. *Neuron* **93**, 480-490. doi:10.1016/j.neuron.2016.12.041
- Kram, R., Wong, B. and Full, R. J. (1997). Three-dimensional kinematics and limb kinetic energy of running cockroaches. *J. Exp. Biol.* **200**, 1919-1929. doi:10.1242/jeb.200.13.1919
- Kuo, A. D. (2007). The six determinants of gait and the inverted pendulum analogy: a dynamic walking perspective. *Hum. Mov. Sci.* **26**, 617-656. doi:10.1016/j.humov.2007.04.003
- Li, C., Pullin, A. O., Haldane, D. W., Lam, H. K., Fearing, R. S. and Full, R. J. (2015). Terradynamically streamlined shapes in animals and robots enhance traversability through densely cluttered terrain. *Bioinspir. Biomim.* **10**, 46003. doi:10.1088/1748-3190/10/4/046003
- Li, C., Kessens, C. C., Fearing, R. S. and Full, R. J. (2017). Mechanical principles of dynamic terrestrial self-righting using wings. *Adv. Robot.* **31**, 881-900. doi:10.1080/01691864.2017.1372213
- Li, J., Orrego, S., Pan, J., He, P. and Kang, S. H. (2019a). Ultrasensitive, flexible, and low-cost nanoporous piezoresistive composites for tactile pressure sensing. *Nanoscale* **11**, 2779-2786. doi:10.1039/C8NR09959F
- Li, C., Wöhrl, T., Lam, H. K. and Full, R. J. (2019b). Cockroaches use diverse strategies to self-right on the ground. *J. Exp. Biol.* **222**, jeb186080. doi:10.1242/jeb.186080
- Lock, R. J., Burgess, S. C. and Vaidyanathan, R. (2013). Multi-modal locomotion: from animal to application. *Bioinspir. Biomim.* **9**, 011001. doi:10.1088/1748-3182/9/1/011001
- Low, K. H., Hu, T., Mohammed, S., Tangorra, J. and Kovac, M. (2015). Perspectives on biologically inspired hybrid and multi-modal locomotion. *Bioinspir. Biomim.* **10**, 020301. doi:10.1088/1748-3190/10/2/020301
- Mathis, A., Mamidanna, P., Cury, K. M., Abe, T., Murthy, V. N., Mathis, M. W. and Bethge, M. (2018). DeepLabCut: markerless pose estimation of user-defined body parts with deep learning. *Nat. Neurosci.* **21**, 1281-1289. doi:10.1038/s41593-018-0209-y
- Mi, J., Wang, Y. and Li, C. (2022). Omni-Roach: a legged robot capable of traversing multiple types of large obstacles and self-righting. *IEEE International Conference on Robotics and Automation (ICRA)*, (in press). Preprint at: <https://arxiv.org/abs/2112.10614>
- Mongeau, J.-M., Demir, A., Lee, J., Cowan, N. J. and Full, R. J. (2013). Locomotion- and mechanics-mediated tactile sensing: antenna reconfiguration simplifies control during high-speed navigation in cockroaches. *J. Exp. Biol.* **216**, 4530-4541. doi:10.1242/jeb.083477
- Mongeau, J.-M., Sponberg, S. N., Miller, J. P. and Full, R. J. (2015). Sensory processing within antenna enables rapid implementation of feedback control for high-speed running maneuvers. *J. Exp. Biol.* **218**, 2344-2354. doi:10.1242/jeb.118604
- Moss, C. F., Bohn, K., Gilkenson, H. and Surlykke, A. (2006). Active Listening for Spatial Orientation in a Complex Auditory Scene. *PLoS Biol.* **4**, e79. doi:10.1371/journal.pbio.0040079
- Nelson, M. E. and MacIver, M. A. (2006). Sensory acquisition in active sensing systems. *J. Comp. Physiol. A* **192**, 573-586. doi:10.1007/s00359-006-0099-4
- Okada, J., Kanamaru, Y. and Toh, Y. (2002). Mechanosensory control of antennal movement by the scapal hair plate in the American Cockroach. *Zool. Sci.* **19**, 1201-1210. doi:10.2108/zsj.19.1201
- Othayoth, R. and Li, C. (2021). Propelling and perturbing appendages together facilitate strenuous ground self-righting. *eLife* **10**, e60233. doi:10.7554/eLife.60233
- Othayoth, R., Thoms, G. and Li, C. (2020). An energy landscape approach to locomotor transitions in complex 3D terrain. *Proc. Natl. Acad. Sci. USA* **117**, 14987-14995. doi:10.1073/pnas.1918297117
- Othayoth, R., Xuan, Q., Wang, Y. and Li, C. (2021). Locomotor transitions in the potential energy landscape-dominated regime. *Proc. R. Soc. B Biol. Sci.* **288**, rspb.2020.2734. doi:10.1098/rspb.2020.2734
- Pearson, K. G. and Iles, J. F. (1973). Nervous mechanisms underlying intersegmental co-ordination of leg movements during walking in the cockroach. *J. Exp. Biol.* **58**, 725-744. doi:10.1242/jeb.58.3.725
- Prescott, T. J., Diamond, M. E. and Wing, A. M. (2011). Active touch sensing. *Philos. Trans. R. Soc. B Biol. Sci.* **366**, 2989-2995. doi:10.1098/rstb.2011.0167
- Ritzmann, R. E., Pollack, A. J., Archinal, J., Ridgel, A. L. and Quinn, R. D. (2005). Descending control of body attitude in the cockroach *Blaberus discoidalis* and its role in incline climbing. *J. Comp. Physiol. A* **191**, 253-264. doi:10.1007/s00359-004-0537-0
- Ritzmann, R. E., Harley, C. M., Daltorio, K. A., Tietz, B. R., Pollack, A. J., Bender, J. A., Guo, P., Horomanski, A. L., Kathman, N. D., Nieuwoudt, C. et al. (2012). Deciding which way to go: how do insects alter movements to negotiate barriers? *Front. Neurosci.* **6**, 1-10. doi:10.3389/fnins.2012.00097
- Sanderson, D. and Jackson, C. F. (1912). *Elementary Entomology*. Boston, MA: Ginn and Company.
- Schilling, M. and Cruse, H. (2020). Decentralized control of insect walking: a simple neural network explains a wide range of behavioral and neurophysiological results. *PLoS Comput. Biol.* **16**, e1007804. doi:10.1371/journal.pcbi.1007804
- Schütz, C. and Dürr, V. (2011). Active tactile exploration for adaptive locomotion in the stick insect. *Philos. Trans. R. Soc. B Biol. Sci.* **366**, 2996-3005. doi:10.1098/rstb.2011.0126
- Shepard, E. L. C., Wilson, R. P., Rees, W. G., Grundy, E., Lambertucci, S. A. and Vosper, S. B. (2013). Energy landscapes shape animal movement ecology. *Am. Nat.* **182**, 298-312. doi:10.1086/671257
- Spence, A. J., Revzen, S., Seipel, J., Mullens, C. and Full, R. J. (2010). Insects running on elastic surfaces. *J. Exp. Biol.* **213**, 1907-1920. doi:10.1242/jeb.042515
- Spirito, C. P. and Mushrush, D. L. (1979). Interlimb coordination during slow walking in the cockroach: I. Effects of substrate alterations. *J. Exp. Biol.* **78**, 233-243. doi:10.1242/jeb.78.1.233
- Sponberg, S. and Full, R. J. (2008). Neuromechanical response of musculo-skeletal structures in cockroaches during rapid running on rough terrain. *J. Exp. Biol.* **211**, 433-446. doi:10.1242/jeb.012385
- Sponberg, S., Spence, A. J., Mullens, C. H. and Full, R. J. (2011a). A single muscle's multifunctional control potential of body dynamics for postural control and running. *Philos. Trans. R. Soc. B Biol. Sci.* **366**, 1592-1605. doi:10.1098/rstb.2010.0367
- Sponberg, S., Libby, T., Mullens, C. H. and Full, R. J. (2011b). Shifts in a single muscle's control potential of body dynamics are determined by mechanical feedback. *Philos. Trans. R. Soc. B Biol. Sci.* **366**, 1606-1620. doi:10.1098/rstb.2010.0368
- Stamper, S. A., Roth, E., Cowan, N. J. and Fortune, E. S. (2012). Active sensing via movement shapes spatiotemporal patterns of sensory feedback. *J. Exp. Biol.* **215**, 1567-1574. doi:10.1242/jeb.068007
- Staudacher, E. M., Gebhardt, M. and Dürr, V. (2005). Antennal movements and mechanoreception: neurobiology of active tactile sensors. *Adv. Insect Physiol.* **32** Suppl. 11, 49-205. doi:10.1016/S0065-2806(05)32002-9
- Theunissen, L. M. and Dürr, V. (2013). Insects use two distinct classes of steps during unrestrained locomotion. *PLoS ONE* **8**, e85321. doi:10.1371/journal.pone.0085321
- Tuthill, J. C. and Azim, E. (2018). Proprioception. *Curr. Biol.* **28**, R194-R203. doi:10.1016/j.cub.2018.01.064
- Tuthill, J. C. and Wilson, R. I. (2016). Mechanosensation and adaptive motor control in insects. *Curr. Biol.* **26**, R1022-R1038. doi:10.1016/j.cub.2016.06.070
- Wang, Y., Othayoth, R. and Li, C. (2021). A robophysical model to study physical sensing of obstacles in legged traversal of complex 3-D terrain. *Bull. Am. Phys. Soc.* **66**, S14.00007.
- Watson, J. T., Ritzmann, R. E. and Pollack, A. J. (2002). Control of climbing behavior in the cockroach, *Blaberus discoidalis*. II. Motor activities associated with joint movement. *J. Comp. Physiol. A Sens. Neural Behav. Physiol.* **188**, 55-69. doi:10.1007/s00359-002-0278-x
- Wöhrl, T., Reinhardt, L. and Blickhan, R. (2017). Propulsion in hexapod locomotion: how do desert ants traverse slopes? *J. Exp. Biol.* **220**, 1618-1625. doi:10.1242/jeb.137505
- Xuan, Q. and Li, C. (2020a). Coordinated appendages accumulate more energy to self-right on the ground. *IEEE Robot. Autom. Lett.* **5**, 6137-6144. doi:10.1109/LRA.2020.3011389
- Xuan, Q. and Li, C. (2020b). Randomness in appendage coordination facilitates strenuous ground self-righting. *Bioinspir. Biomim.* **15**, 065004. doi:10.1088/1748-3190/abac47
- Xuan, Q., Wang, Y. and Li, C. (2022). Environmental force sensing enables robots to traverse cluttered obstacles with interaction. *arXiv*, 2112.2112.07900 [cs.RO].
- Zheng, B., Xuan, Q. and Li, C. (2022). A minimalistic stochastic dynamics model of cluttered obstacle traversal. *IEEE Robot. Autom. Lett.* **7**, 5119-5126. doi:10.1109/LRA.2022.3150831

## Supplementary Materials and Methods

### Minimal mechanical energetic cost in pitch and roll mode

To quantify how strenuous the pitch and roll modes are, we estimated the minimal mechanical energetic cost of the pitch or roll mode by calculating the maximal potential energy increase of the system during the traversal process using either mode.

For the pitch mode, we assumed that the animal kept a horizontal body orientation (zero body pitch and roll, neglecting legs), moved forward in the middle of the two beams with the lowest point of the body always contacting the ground, and pushed the beams down to traverse. The maximal potential energy increase of 7.9 mJ occurred when both beams deflected by nearly 90°.

For the roll mode, we assumed that the animal started with a horizontal body orientation and rolled by 90° to move through between the beams without deflecting them, with the lowest point of the body always contacting the ground. The maximal potential energy increase of 0.2 mJ occurred when the body roll was 90°.

### S2. Pitch-to-roll transition barrier

The pitch-to-roll transition barrier can be calculated from the potential energy landscape model, and it is a function of the forward position  $x$  (Othayoth et al., 2020). In our previous study that used a simple ellipsoid to model the animal, when traversing beams of  $K = 1.7 \text{ mN}\cdot\text{m}\cdot\text{rad}^{-1}$ , the pitch-to-roll transition barrier was 0.04 mJ at  $x = -21 \text{ mm}$  where the animal was observed to transition ((Othayoth et al., 2020), Fig. 6B, iv), and it was 0.0021 mJ at  $x = -13.6 \text{ mm}$ . In this study that used a refined animal model, when traversing beams of  $K = 2.5 \text{ mN}\cdot\text{m}\cdot\text{rad}^{-1}$ , the pitch-to-roll transition barrier was 0.052 mJ at  $x = -21 \text{ mm}$ ,

and it was 0.0027 mJ at  $x = -13.6$  mm where the animal transitioned. These similar values between the two studies demonstrated that our potential energy landscape approach is consistent and useful either with the simplest or refined animal model.

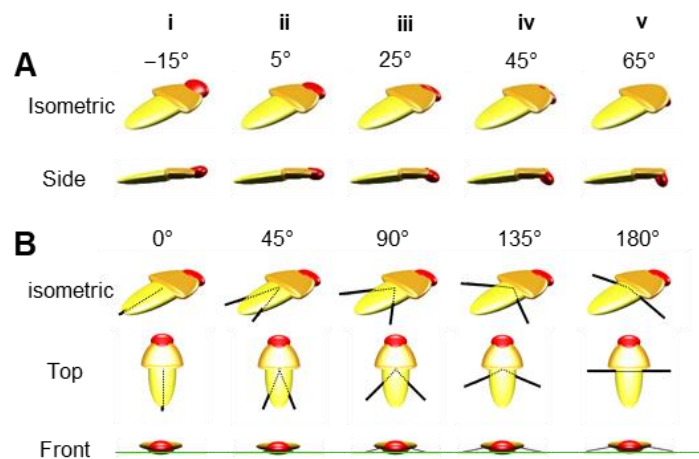


**Fig. S1. Example variation of head flexion and total leg sprawl to test the use of head and leg adjustments in potential energy landscape model. (A) Head flexion. (B) Total leg sprawl.**

Green line in (B) front view is leg height = -5 mm.

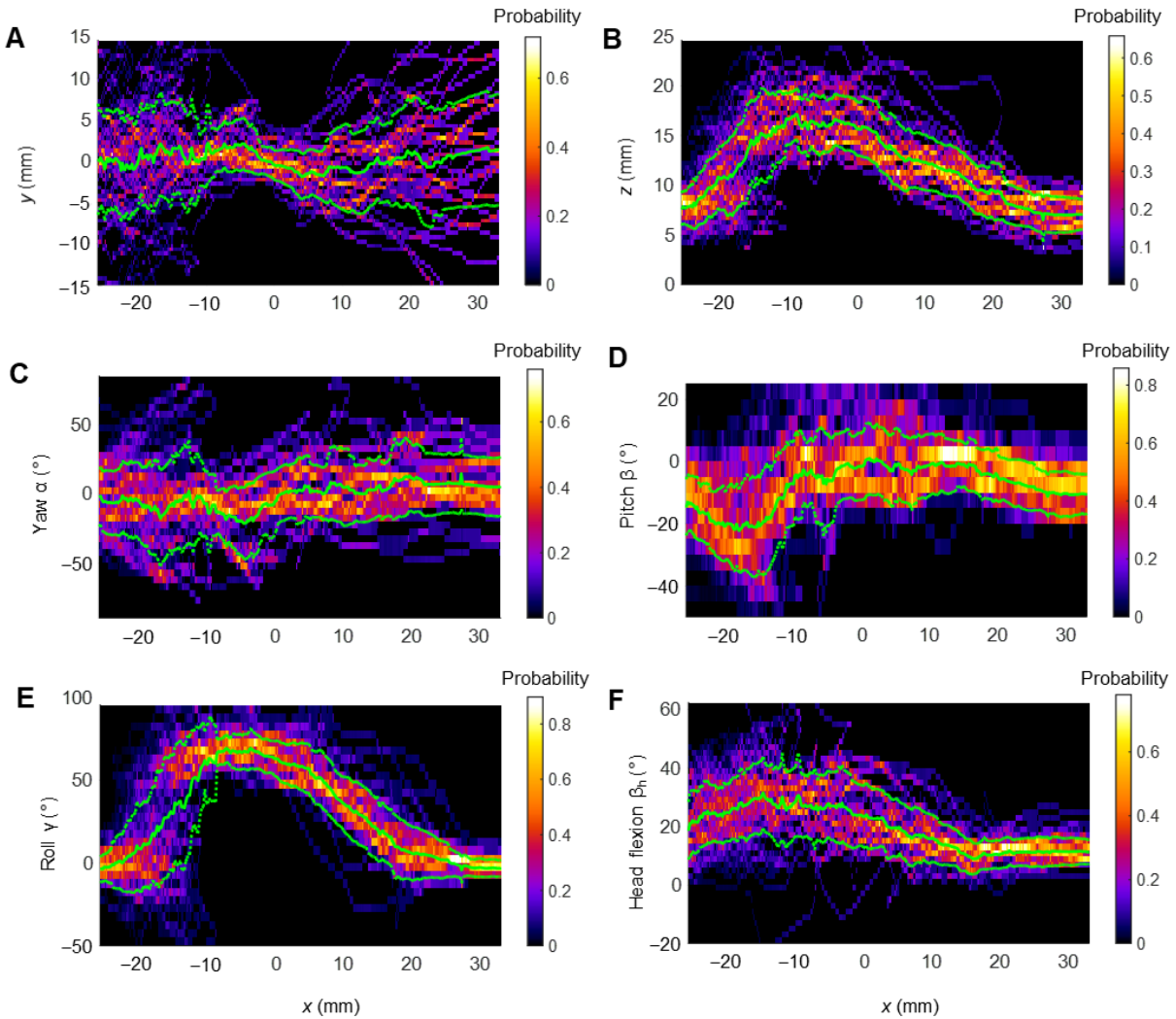


**Fig. S2. Average trajectory as a function of forward position  $x$ .** (A) Lateral position  $y$ . (B) Vertical position  $z$ . (C) Yaw  $\alpha$ . (D) Pitch  $\beta$ . (E) Roll  $\gamma$ . (F) Head flexion  $\beta_h$ . Solid and dashed green curves are mean  $\pm$  s.d. from averaging data of all trials. Each column of the heat map is a normalized histogram showing probability distribution of the data (sum of each column is 1) at corresponding forward position  $x$ .

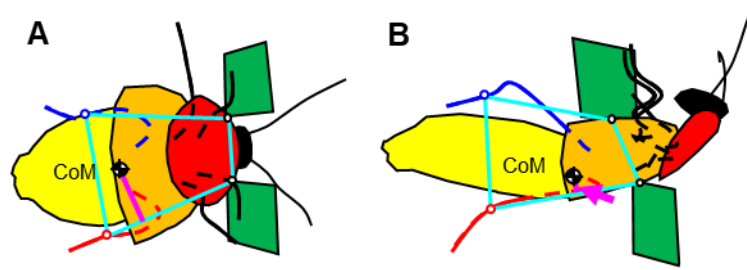


**Fig. S3. Representative support polygon evolution from top view during pitch-to-roll transition.** (A) Explore + pitch phases. (B) Roll phase. Cyan closed shapes show support polygons, and magenta lines show the distance from center of mass (CoM) to nearest lateral edge of the support polygon, which measures roll stability. In (B), the distance is small and indicated by a magenta arrow.

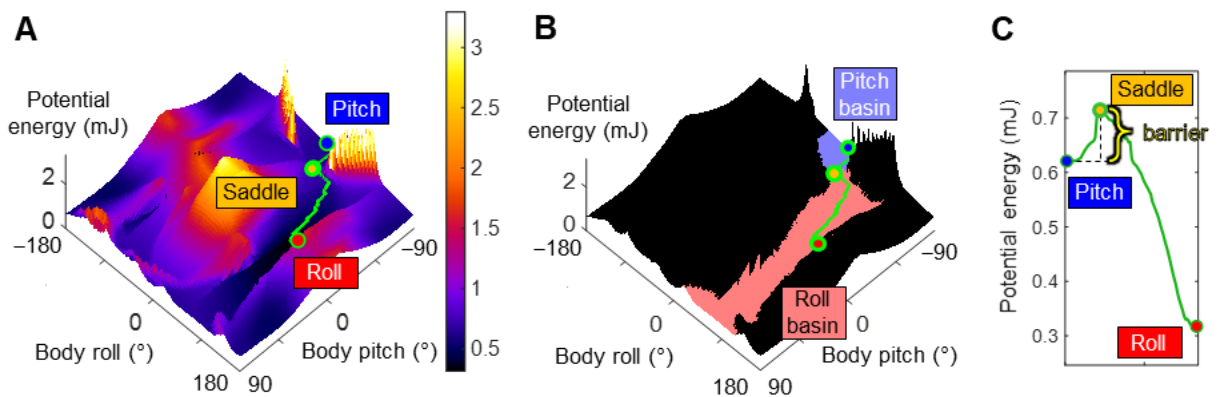


**Fig. S4. Demonstration of breath-first search result on potential energy landscape.** (A) Potential energy landscape pitch-roll cross section at  $x = 0$  along the average animal trajectory, with hind legs neglected. Blue and red dots are pitch and roll local minima, respectively. Orange dot is saddle point. Green curve is imaginary route obtained from parent backtracking (Sec. 2.11). (B) Basins identified from breath-first search. Blue and red areas are pitch and roll basins, respectively. Boundary of basins is iso-height contour with the same potential energy as saddle point. Black area is rest of landscape. (C) Potential energy along imaginary route. Potential energy barrier is increase in potential energy from pitch minimum to saddle point. Note that imaginary route is only for defining saddle point, and during transition, animal did not necessarily start from a local minimum or transition by crossing saddle point.

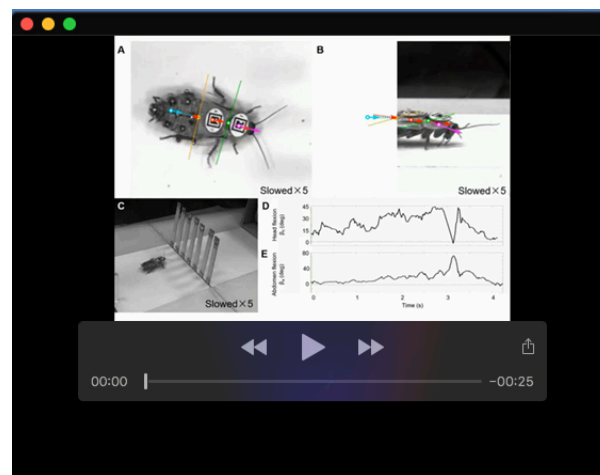
**Table S1. Ranges and increment of variables used in initial landscape variation (sweep) and the dimension collapse protocols used in subsequent pitch-roll and yaw cross-section analyses**

Variable	Unit	Min	Max	Increment	Dimension collapsing protocol	
					Pitch-roll cross-section	Yaw cross-section
Forward position $x$	mm	-26	33	0.2	Not collapsed	Not collapsed
Lateral position $y$	mm	-3	3	1	Follow average trajectory	Follow average trajectory
Vertical position $z$	mm	$z_{\min}$	$z_{\min} + 1$	1	Minimize potential energy	Minimize potential energy
Yaw $\alpha$	deg	-90	90	5	Follow average trajectory	Not collapsed
Pitch $\beta$	deg	-90	90	2	Not collapsed	Follow average trajectory
Roll $\gamma$	deg	-180	180	2	Not collapsed	Follow average trajectory
Head flexion $\beta_h$	deg	-25	65	5	Not collapsed or follow average trajectory	Not collapsed
Abdomen flexion $\beta_a$	deg	7	7	-	-	-

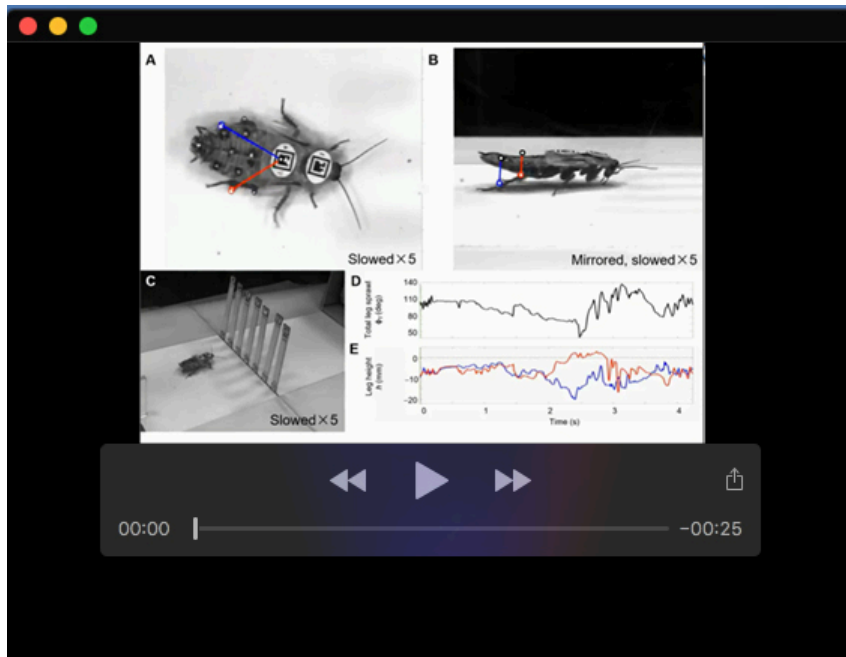
$z_{\min}$ : vertical position  $z$  when the body touched the ground.

**Table S2. Frequently used averaged variables in landscape analyses**

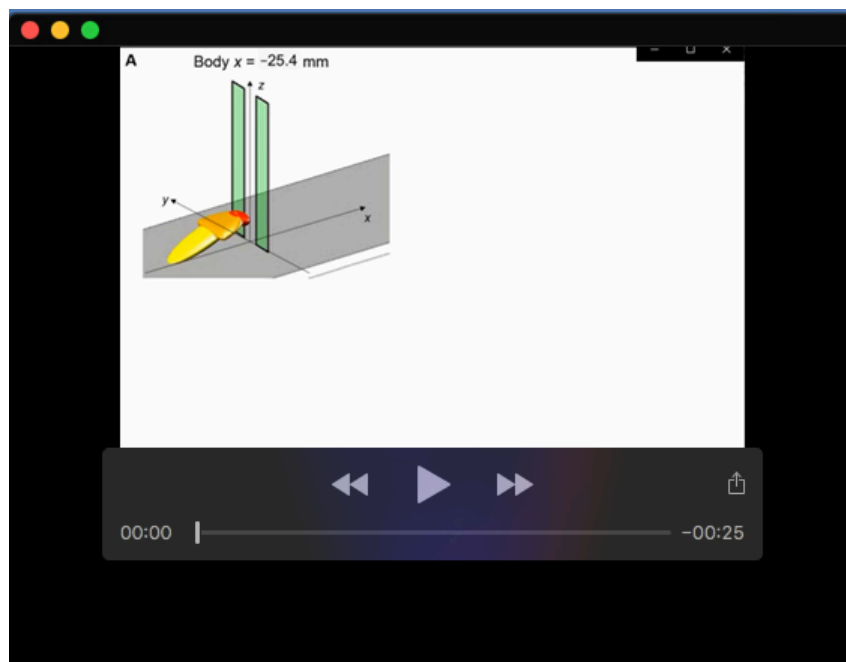
Variable	Time range	Measured value	Used value
Forward position $x$	Pitch-to-roll transition	$-13.6 \pm 4.4$ mm	-13.6 mm
Maximum leg length	Explore + pitch and roll phase	$27 \pm 2$ mm	27 mm
Temporal averaged abdomen flexion $\beta_a$	Approach phase	$7^\circ \pm 4^\circ$	$7^\circ$
Head flexion range $\beta_h$	Whole trial	$[-24^\circ, 64^\circ]$	-
Temporal averaged head flexion $\beta_h$	Approach phase	$15^\circ \pm 4^\circ$	$15^\circ$
Temporal averaged leg height	Explore + pitch phase	$-5 \pm 3$ mm	-5 mm
Maximal total leg sprawl $\phi_T$	Explore + pitch phase	$156^\circ \pm 21^\circ$	$160^\circ$
Minimal total leg sprawl $\phi_T$	Roll phase	$21^\circ \pm 17^\circ$	$20^\circ$
Kinetic energy fluctuation	Explore + pitch and roll phase	$0.01 \pm 0.01$ mJ	0.01 mJ
Temporal averaged forward position $x$	Explore + pitch phase	$-20 \pm 3$ mm	-20 mm



**Movie 1.** Head and abdomen flexion. Top: zoomed top (left) and side (right) views. White points with red, magenta, cyan, green, and orange edges are the origins of thorax frame, head frame, abdomen frame, middle point of thorax-head joint, and middle point of the thorax-abdomen joint, respectively. Solid and dotted arrows show  $+x$  and  $+x'$  direction of body (red), head (magenta), and abdomen (cyan) frames, respectively. Head and abdomen flexion are the angles between body  $+x'$  direction and head or abdomen  $+x$  direction. Bottom left: isometric view. Bottom right: head and abdomen flexion as a function of time.



**Movie 2.** Leg adjustments. Top left: zoomed top view. White points with thick blue, red, and black edges are the left and right tibia-tarsal joints and origin of thorax frame, respectively. White points with thin blue and red edges are the projections of the tibia-tarsal joints into the body coronal plane. Total leg sprawl is the angle between the dashed blue and red lines. Top right: zoomed mirrored side view. White points with blue, red, and black edges are tibia-tarsal joints and their projections to body coronal plane, respectively. Leg height of left and right hind legs is opposite value of the length of the blue and red lines, respectively. Bottom left: isometric view. Note that this view is mirrored to better show leg motion. Bottom right: Leg sprawl (top) and leg height (bottom) as a function of time. Blue and red are for left and right hind legs, respectively.



**Movie 3.** Potential energy landscape model. Part 1. Pitch-to-roll transition on pitch-roll cross section. Part 2. Roll-to-deflect transition on yaw cross section. Top left: model of cockroach traversing beam obstacles at head flexion  $\beta_h = 15^\circ$  with hind legs neglected. Top right: potential energy landscape pitch-roll cross section (part 1) or yaw cross section (part 2) along the average animal trajectory. Blue, red, and purple dots are pitch, roll, and deflect local minima, respectively. Orange dots are saddle points. Green curves are imaginary routes. Bottom left: Potential energy along the imaginary route. Bottom right: Potential energy barrier as a function of forward position  $x$ .